Riemann problem for kinematical conservation laws and geometrical features of nonlinear wavefronts

S. Baskar and Phoolan Prasad*

Abstract

A pair of kinematical conservation laws (KCL) in a ray coordinate system (ξ, t) are the basic equations governing the evolution of a moving curve in two space-dimensions. We first study elementary wave solutions and then the Riemann problem for KCL when the metric g, associated with the coordinate ξ designating different rays, is an arbitrary function of the velocity of propagation m of the moving curve. We assume that $m > 1$ (m is appropriately normalized), for which the system of KCL becomes hyperbolic. We interpret the images of the elementary wave solutions in the (ξ, t)-plane to the (x, y)-plane as *elementary shapes* of the moving curve (or a nonlinear wavefront when interpreted in a physical system) and then describe their geometrical properties. Solutions of the Riemann problem with different initial data give the shapes of the nonlinear wavefront with different combinations of elementary shapes. Finally, we study all possible interactions of elementary shapes.

1 Introduction

Consider a one parameter family of curves in (x, y)-plane such that they represent successive positions of a moving curve Ω_t as time t varies. Associated with the family, we have a ray velocity $\boldsymbol{\chi}$ at any point (x, y) on the curve Ω_t. We take $\boldsymbol{\chi}$ to be in the direction of the unit normal $\boldsymbol{n}$ to Ω_t i.e., $\boldsymbol{\chi} = \boldsymbol{n}C$; where C is the normal velocity of propagation of Ω_t. We introduce a ray coordinate system (ξ, t) such that $\xi =$ constant represent the rays i.e., the family of curves orthogonal to Ω_t and $t =$ constant give successive positions of Ω_t. An element of distance along a ray is given by Cdt. Let g be the metric associated with the coordinate ξ i.e., $gd\xi$ is the element of distance along Ω_t. Assuming Ω_t to be smooth, and taking $\boldsymbol{n} = (\cos\theta, \sin\theta)$, Morton, Prasad and Ravindran (1992) derived a pair of conservation laws

$$(g\sin\theta)_t + (C\cos\theta)_\xi = 0, \tag{1.1}$$

$$(g\cos\theta)_t - (C\sin\theta)_\xi = 0. \tag{1.2}$$

* Department of Mathematics, Indian Institute of Science, Bangalore 560012. **Email: prasad@math.iisc.ernet.in** (presently at Centre for Plasma-Astrophysics, Department of Mathematics, K U Leuven, Celestijnenlaan 200B, 3001, Leuven.)

The kinematical conservation laws (KCL) (1.1)-(1.2) are physically realistic in the sense that they represent conservation of distance in x and y directions and hence in any two independent directions (Monica and Prasad 2001; Prasad, 2001). The KCL, being two equations in three unknowns g, θ and C, is an under determined system. The third equation (or larger number of equations, Monica and Prasad, 2001) involving g and C (or some more quantities) are obtained by consideration of energy propagation along rays (or from dynamical compatibility conditions along rays for a given physical system; Prasad, 2001). Here we take a simpler view and assume that the flux of energy $F(C)$ associated with the moving curve Ω_t (or the wavefront Ω_t) is the same at each section of a ray tube by Ω_t resulting in a third conservation law

$$(gF(C))_t = 0. \tag{1.3}$$

This leads to a complete system of three conservation laws (1.1)-(1.3) describing evolution of a propagating curve Ω_t. Linear wave propagation in a nonlinear medium such as a polytropic gas correspond to small amplitude perturbation and hence carries vanishingly small energy density. Let us consider a nonlinear wave propagation in the medium which is assumed to be isotropic and homogeneous with a constant local sound speed a_0 ahead of the wave. Isotropy is equivalent to our basic assumption that rays are orthogonal to the successive positions of the curves Ω_t. We now nondimensionalize all variables with respect to an appropriate length scale L and time scale La_0^{-1} and define a Mach number of Ω_t by $m = C/a_0$. It is found in some examples (see (1.8) and (1.9) below) that

$$\lim_{m\to 1+} G(m) = \infty, \text{ where } G(m) = 1/F(m). \tag{1.4}$$

From now onwards, all dependent and independent variables are nondimensional so that $C = m$. Even for an isotropic case, derivation (1.3) is difficult mainly due to difficulty in capturing the nonlinear rays in a perturbation method (Prasad, 2001, chapter 4). The transport equation (1.3) is then derived along these nonlinear rays. Derivation of an expression for $F(m)$ is equally difficult (see Baskar and Prasad, 2001) when Ω_t is the crest-line of a curved solitary wave.

It has been shown (Prasad, 1995) [1] that the KCL (1.1)-(1.2), derived purely on geometric considerations, are equivalent to the ray equations derived from the eikonal equation

$$\phi_t + m|\nabla\phi| = 0. \tag{1.5}$$

The first two of the three ray equations derived from the eikonal equation (1.5) are

$$x_t = m\cos\theta, \quad y_t = m\sin\theta. \tag{1.6}$$

[1] All results, obtained previously by us, are available in the book by Prasad (2001), however we shall refer to individual papers.

The third ray equation (second equation in (2.5) in the next section) follows from the transport equations for ϕ_x or ϕ_y in the characteristic equations of (1.5) (see Prasad, 2001, equation (2.4.25) with $\boldsymbol{q} = \mathbf{0}$). $g^2 = x_\xi^2 + y_\xi^2$ and (1.6) lead to the equation for g (third equation in (2.5)). For more details, see Prasad (2001, section 3.3.2).

The KCL are ideally suited to describe kinks on the propagating curve Ω_t (Prasad, 1995), which are images of shocks (in weak solutions of the KCL) in (ξ, t)-plane to (x, y)-plane under the transformation (1.6). At a kink in (x, y)-plane, the tangent direction to Ω_t and the wave amplitude m along Ω_t change discontinuously. Kinks were first noticed by Whitham (1974) as shock-shocks, in his shock dynamics. There are two more relations, which follows from geometrical consideration, namely

$$x_\xi = -g\sin\theta, \quad y_\xi = g\cos\theta. \tag{1.7}$$

It is interesting to note that the KCL follow from (1.6) and (1.7) simply by equating $x_{\xi t} = x_{t\xi}$ and $y_{\xi t} = y_{t\xi}$.

From our weakly nonlinear ray theory (WNLRT) in gas dynamics, we derived (Morton, Prasad and Ravindran, 1992; Prasad, 1993) an expression for g in terms of m in the form

$$g = (m-1)^{-2}e^{-2(m-1)}. \tag{1.8}$$

When Ω_t represents the crest-line of a curved solitary wave on the surface of a shallow water, we have shown (Baskar and Prasad, 2001) that

$$g = (m-1)^{-\frac{3}{2}}e^{-\frac{3}{2}(m-1)}. \tag{1.9}$$

For the solitary wave, we can deduce more than one expression for g, one of them being $g = (m-1)^{-1}e^{-(m-1)}$ but only (1.9) is physically realistic. Note that both examples are valid for small positive values of $m-1$. The system (1.1)-(1.2) together with a relation between g and m is now closed and hence the energy conservation law (1.3) is no longer required.

When sonic boom from an accelerating aircraft is traced via linear rays, the rays tend to converge to envelop a caustic line or meet at a focus. Beyond the region bounded by the caustic line, called focal zone, linear solutions are singular, whereas the actual (experimental) solution has finite amplitude with a u-wave shape due to nonlinear effects. Plotkin (2001), in his recent review on sonic booms mentioned various methods to calculate the solution in focal zones. The kinematical conservation law discussed above is yet another method to handle this problem, as it is evident from the numerical solutions of KCL obtained by Prasad and Sangeeta (1996). The KCL can also be used more effeciently to many other applications such as in finding the shape of the leading wavefront in the blast wave problem produced

by a charge confined in a container of arbitrary shape, studying geometrical shapes of the crest-line on a curved solitary wave on a shallow water (Baskar and Prasad, 2002) and so on. In different applications, we may need to solve the KCL with different functions $G(m)$ and with different initial wavefronts. So, a mathematical theory is needed for KCL with an arbitrary $G(m)$ for a better understanding of the practical problems. The Riemann problem and the interaction of elementary waves are the building blocks for the general mathematical theory of hyperbolic conservation laws and hence it is important to study the solution of the Riemann problem and the interaction of the elementary waves for the KCL.

In this paper we shall also examine the situation when a relation of the form $g = G(m)$ can be assumed to be uniformly valid i.e., valid across all possible discontinuities. However, our main aim in this paper is to solve the Riemann problem for the system of conservation laws (1.1)-(1.3) with a general expression for $G(m)$ subject to certain assumptions and interpret the results as geometrical features of the moving curve Ω_t (or a nonlinear wavefront). The solution of the Riemann problem will lead to a number of elementary shapes (to be defined later) on Ω_t separated by straight parts of Ω_t. In the last section we shall discuss interaction of two elementary shapes of Ω_t giving rise to new elementary shapes. This results in beautiful geometrical features of Ω_t and vastly extend incomplete results of Baskar, Potdar and Szeftel (1999) with g given by (1.8).

2 Basic Equations, Riemann invariants and jump relations

We write the three basic conservation laws (1.1)-(1.3) in vector form as

$$(\boldsymbol{H}(\boldsymbol{u}))_t + (\boldsymbol{F}(\boldsymbol{u}))_\xi = 0, \tag{2.1}$$

where $\boldsymbol{u} := (\boldsymbol{v}, g)^T = (m, \theta, g)^T$, so that $\boldsymbol{v} = (m, \theta)^T$ and

$$\boldsymbol{H}(\boldsymbol{u}) := (g\sin\theta, g\cos\theta, g/G(m))^T, \tag{2.2}$$

$$\boldsymbol{F}(\boldsymbol{u}) := (m\cos\theta, -m\sin\theta, 0)^T. \tag{2.3}$$

We assume that the function $G(m)$ given in (1.4) is defined for $m > 1$ and satisfies:

A1. $G(m) \sim \frac{1}{(m-1)^k}$, $k > 0$ for $0 < m - 1 \ll 1$.
A2. $\lim_{m\to\infty} G(m) = 0$; $G(m) > 0$.
A3. $G'(m) < 0$.
A4. $G''(m) > 0$.

These properties are satisfied by the functions (1.8)-(1.9). Since, some of the results we use in the section 6 are very difficult to prove (they involve dealing with nonlinear functions),

we verify those results numerically. For this purpose, we select a form for $G(m)$ as

$$G(m) = (m-1)^{-k} e^{-n(m-1)},\ k > 0, n > 0, \text{ for all } m > 1. \tag{2.4}$$

Since

$$G' = -\frac{k + n(m-1)}{m-1} G(m), \quad G''(m) = \left\{ \frac{k(k+1)}{(m-1)^2} + \frac{2kn}{m-1} + n^2 \right\} G(m),$$

the above four assumptions are satisfied by (2.4).

For a smooth solution, the system (2.1)-(2.3) is equivalent to the following three partial differential equations

$$m_t - \frac{mG}{gG'}\theta_\xi = 0, \quad \theta_t + \frac{1}{g} m_\xi = 0, \quad g_t - m\theta_\xi = 0. \tag{2.5}$$

The eigenvalues of the system (2.5) are given by

$$c_1 = -\sqrt{\frac{mG}{g^2(-G')}}, \quad c_2 = 0, \quad c_3 = \sqrt{\frac{mG}{g^2(-G')}}. \tag{2.6}$$

From the assumption **A3**, it follows that the system (2.1)-(2.3) is hyperbolic for $m > 1$. For WNLRT in a polytropic gas, $m > 1$ corresponds to the gas pressure on the wavefront Ω_t being greater than the pressure in the ambient medium in which Ω_t is propagating and for a solitary wave on a shallow water, $m > 1$ always holds.

The right eigenvectors corresponding to the eigenvalues (2.6) are

$$\boldsymbol{r}^{(1)} = \left(\frac{G}{gG'}, \sqrt{\frac{G}{mg^2(-G')}}, 1 \right)^T, \quad \boldsymbol{r}^{(2)} = (0, 0, 1)^T,$$
$$\boldsymbol{r}^{(3)} = \left(\frac{G}{gG'}, -\sqrt{\frac{G}{mg^2(-G')}}, 1 \right)^T.$$

The c_1 - and c_3 - characteristic fields are genuinely nonlinear, and the c_2-characteristic field is linearly denerate (for basic definitions, we refer to Smoller, 1983 or Prasad, 2001). Thus, there are two families of nonlinear waves and one family of linear waves which propagate on the curve Ω_t in the (x, y)-plane. The elementary wave solutions of the system of conservation laws will consists of centered simple waves, shocks and contact discontinuities, which we shall study in the next section.

The linearly independent Riemann invariants corresponding to the ith characteristic fields are denoted by $(\pi_1^{(i)}, \pi_2^{(i)})$ for $i = 1, 2, 3$ and are given by

$$\pi_1^{(1)} = \theta + L(m),\ \pi_2^{(1)} = \frac{g}{G};\ \pi_1^{(2)} = m,\ \pi_2^{(2)} = \theta;\ \pi_1^{(3)} = \theta - L(m),\ \pi_2^{(3)} = \frac{g}{G}, \tag{2.7}$$

where

$$L(m) = \int_1^m \sqrt{\frac{-G'}{mG}}dm. \tag{2.8}$$

Let the subscripts l and r represent the values of the solution on the left and the right of a discontinuity at $\xi_s(t)$ and s be the discontinuity velocity $s = d\xi_s(t)/dt$. Then, from the Rankine-Hugoniot jump condition for the KCL (1.1)-(1.2) (see Prasad, 1995), we get

$$\cos(\theta_r - \theta_l) = \frac{m_l g_l + m_r g_r}{m_l g_r + m_r g_l}, \tag{2.9}$$

$$s(g_l G(m_r) - g_r G(m_l)) = 0. \tag{2.10}$$

The discontinuity velocity speed s is given by

$$s = \frac{(m_r^2 - m_l^2)}{(m_l g_r + m_r g_l)\sin(\theta_r - \theta_l)}. \tag{2.11}$$

When $s \neq 0$, (2.10) implies

$$g_l G(m_r) - g_r G(m_l) = 0 \tag{2.12}$$

and the relation (2.9) becomes

$$\cos(\theta_r - \theta_l) = \frac{m_l G(m_l) + m_r G(m_r)}{m_l G(m_r) + m_r G(m_l)}. \tag{2.13}$$

It has been shown in Lemma 3.1 in the next section that the right hand side of (2.13) belongs to $(0, 1]$ for $m_r \in [1, \infty)$. Therefore, for a given θ_l, the value of θ_r satisfies

$$-\frac{\pi}{2} < \theta_r - \theta_l < \frac{\pi}{2}. \tag{2.14}$$

For this range of value for $\theta_r - \theta_l$, we can write (2.13) as

$$\theta_r - \theta_l = \pm \cos^{-1}\left(\frac{m_l G(m_l) + m_r G(m_r)}{m_l G(m_r) + m_r G(m_l)}\right) = \pm h(m_l, m_r) \text{ (say)}, \tag{2.15}$$

where we take only the positive determination of the $\cos^{-1}$ function. However, we shall see later that a shock transition is possible only for $-\pi/2 < \theta_r - \theta_l < 0$.

3 Elementary wave solutions; existence and uniqueness of rarefaction and Hugoniot curves

Elementary wave solutions of conservation laws (2.1)-(2.3) are the non-constant parts of solutions of the form $m(\xi, t) = m(\xi/t)$, $\theta(\xi, t) = \theta(\xi/t)$, $g(\xi, t) = g(\xi/t)$. These are centered rarefaction wave solutions centered at the origin, shocks and contact discontinuity passing

through the origin. We shall discuss in this section all states which can be joined by an elementary wave solution to a state $\boldsymbol{u}_l$ on the left of it. Without loss of generality we shall take $\theta_l = 0$ in all figures of this paper so that $\boldsymbol{u}_l = (m_l, 0, g_l)$ i.e., $\boldsymbol{v}_l = (m_l, 0)^T$.

The centered rarefaction waves can exist in the first and third characteristic fields and we denote them as 1-R and 3-R waves. In 1-R wave, the two Riemann invariants $\pi_1^{(1)}$ and $\pi_2^{(1)}$ are constants. Therefore, from (2.7), we get

$$\theta^-(m) = \theta_+^* - \int_1^m \sqrt{\frac{-G'(m)}{mG(m)}} dm, \ 1 < m < \infty \tag{3.1}$$

with

$$\theta_+^* = \theta_l + \int_1^{m_l} \sqrt{\frac{-G'(m)}{mG(m)}} dm. \tag{3.2}$$

Similarly, in 3-R wave, the two Riemann invariants $\pi_1^{(3)}$ and $\pi_2^{(3)}$ are constants and hence we have from (2.7)

$$\theta^+(m) = \theta_-^* + \int_1^m \sqrt{\frac{-G'(m)}{mG(m)}} dm, \ 1 < m < \infty \tag{3.3}$$

with

$$\theta_-^* = \theta_l - \int_1^{m_l} \sqrt{\frac{-G'(m)}{mG(m)}} dm. \tag{3.4}$$

Assumption **A2** and **A3** implies that the integrands defining the two functions in (3.1) and (3.3) are continuous for $m > 1$ and from **A1**, it follows that these integrals exists. The leading order terms of these two functions for $0 < m - 1 \ll 1$ are

$$\theta^- - \theta_+^* = -2k^{1/2}(m-1)^{1/2}, \quad \theta^+ - \theta_-^* = 2k^{1/2}(m-1)^{1/2}.$$

Therefore the curve $\theta = \theta^-(m)$, $m > 1$ in (m, θ)-plane touches the line $m = 1$ at $(1, \theta_+^*)$ and approaches this point as $m \to 1+$ from below. We denote this curve by $R_1(\boldsymbol{v}_l)$ and call it the *rarefaction curve* of the first family. Similarly, curve $\theta = \theta^+(m)$, $m > 1$ touches the line $m = 1$ at $(1, \theta_-^*)$ and approaches this point as $m \to 1+$ from above. We denote this curve, the *rarefaction curve* of the third family, by $R_3(\boldsymbol{v}_l)$. The above approximate expressions for $0 < m - 1 \ll 1$ shows that $R_1(\boldsymbol{v}_l)$ and $R_3(\boldsymbol{v}_l)$ are locally lower and upper parts of the parabolas $m - 1 = \frac{1}{4k}\left(\theta - \theta_+^*\right)^2$ and $m - 1 = \frac{1}{4k}\left(\theta - \theta_-^*\right)^2$ respectively. Each of the $R_1(\boldsymbol{v}_l)$ (and $R_3(\boldsymbol{v}_l)$) family of curves depend on θ_l and m_l through a single parameter θ_+^* (and θ_-^*). We can also see that, for any point $\boldsymbol{v}_l'$ in the (m, θ)-plane, $R_1(\boldsymbol{v}_l')$ (and $R_3(\boldsymbol{v}_l')$) can be obtained from $R_1(\boldsymbol{v}_l)$ (and $R_3(\boldsymbol{v}_l)$) simply by translation in the direction of θ axis. Both curves $R_1(\boldsymbol{v}_l)$ and $R_3(\boldsymbol{v}_l)$ pass through the point $\boldsymbol{v}_l = (m_l, \theta_l)$ in (m, θ)-plane as shown in Fig. 3.1. It can be directly seen from (3.1)-(3.4) that the $R_1(\boldsymbol{v}_l)$ and $R_3(\boldsymbol{v}_l)$ curves are strictly monotonic. We note that for a particular G in (2.4),

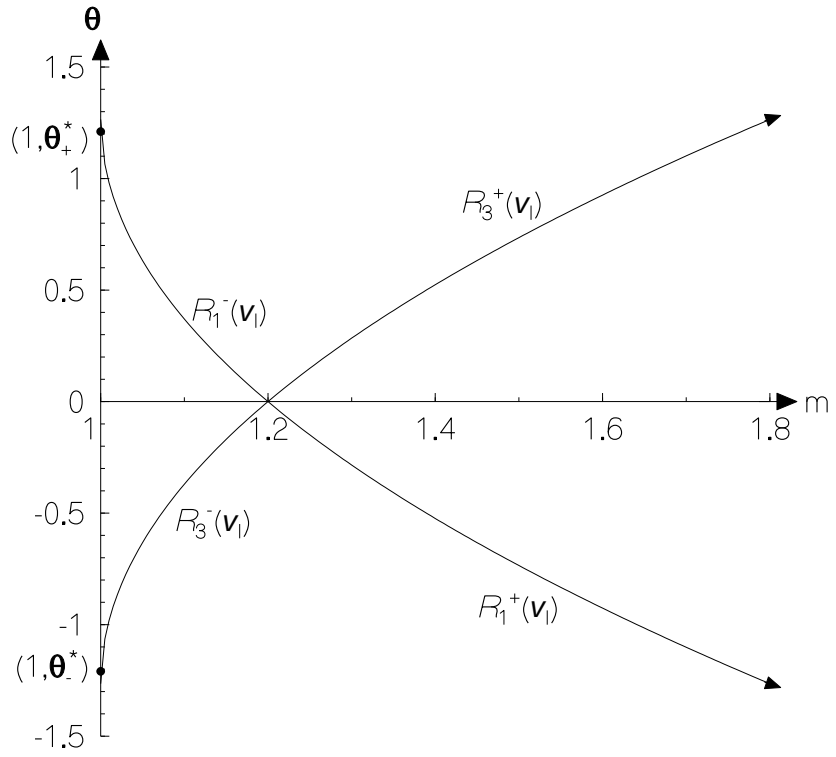

Fig 3.1: *Rarefaction curve* $R_1(\boldsymbol{v}_l) = R_1^+(\boldsymbol{v}_l) \cup R_1^-(\boldsymbol{v}_l) \cup \{\boldsymbol{v}_l\}$ *of first family and* $R_3(\boldsymbol{v}_l) = R_3^+(\boldsymbol{v}_l) \cup R_3^-(\boldsymbol{v}_l) \cup \{\boldsymbol{v}_l\}$ *of third family for* $m_l = 1.2$ *with* $\theta_l = 0$.

$$\left(\theta^-(m)\right)'' = -\left(\theta^+(m)\right)'' = \frac{1}{2}\frac{(2m-1)k + (m-1)^2 n}{m^{3/2}(m-1)^{3/2}}.$$

Since k and n are assumed to be strictly positive, $R_1(\boldsymbol{u}_l)$ is convex and $R_3(\boldsymbol{u}_l)$ is concave.

Let us consider a 1-R wave joining constant states $\boldsymbol{u}_l$ on the left and $\boldsymbol{u}_r$ on the right. Let $\boldsymbol{u}$ be the state on a straight characteristic in the 1-R wave, then from the condition $c_1(\boldsymbol{u}_l) \leq c_1(\boldsymbol{u})$ and $\pi_2^{(1)}(\boldsymbol{u})$=$\pi_2^{(1)}(\boldsymbol{u}_l)$, we get

$$g/G(m) = g_l/G(m_l), \tag{3.5}$$

and

$$\frac{m_l}{G(m_l)(-G'(m_l))} > \frac{m}{G(m)(-G'(m))}. \tag{3.6}$$

Since $G(m)$ and $(-G'(m))$ are decreasing functions of m, $m/(G(m)(-G'(m)))$ is an increasing function of m, the above inequality implies that $m_l > m$. Hence, $\pi_1^{(1)}$=constant in 1-R wave shows that all states in it lie on a part $R_1^-(\boldsymbol{v}_l)$ of the $R_1(\boldsymbol{v}_l)$ in the (m, θ)-plane, where $R_1^-(\boldsymbol{v}_l)$ is given by

$$R_1^-(\boldsymbol{v}_l) = \left\{(m, \theta)/\theta \in \theta^-(m), 1 < m < m_l\right\}. \tag{3.7}$$

Thus, on $R_1^-(\boldsymbol{u}_l)$ curve, we have

$$\theta = \theta_l + \int_m^{m_l} \sqrt{\frac{-G'}{mG(m)}} dm, \quad 1 < m < m_l. \tag{3.8}$$

This gives a value of $\theta > \theta_l$ and the curve $R_1^-(\boldsymbol{v}_l)$ is above the line $\theta = \theta_l$ with $1 < m < m_l$ (see Fig. 3.1). For a given $\boldsymbol{v}_r$ on $R_1^-(\boldsymbol{v}_l)$, the points (m, θ), $m_r < m < m_l$ and $\theta_l < \theta < \theta_r$, on $R_1^-(\boldsymbol{v}_l)$ give the states in a 1-R wave. The arguments given above show that for every $\boldsymbol{v}_l$ with $m_l > 1$ and for G satisfying the assumptions **A1**-**A4** of the section 2, the curve $R_1(\boldsymbol{u}_l)$ is uniquely determined. In particular, if $\boldsymbol{v}_r$ lies on the curve $R_1^-(\boldsymbol{v}_l)$, we get an unique 1-R centered wave joining a constant state $\boldsymbol{v}_l$ on the left and a state $\boldsymbol{v}_r$ on the right.

Consider now a 3-R wave joining a constant state $\boldsymbol{u}_l$ on the left to a state $\boldsymbol{u}_r$ on the right so that $\pi_1^{(3)}(\boldsymbol{u}_l) = \pi_1^{(3)}(\boldsymbol{u}_r)$ and $\pi_2^{(3)}(\boldsymbol{u}_l) = \pi_2^{(3)}(\boldsymbol{u}_r)$. Since the Riemann invariants $\pi_2^{(1)}$ and $\pi_2^{(3)}$ are the same, the intermediate states $\boldsymbol{u} = (m, \theta, g)$ satisfy the relation (3.5) and an additional relation from the constant value of $\pi_1^{(3)}$. Considering the slope of the characteristics of the third family in a 3-R wave (these are straight lines passing through the origin), we deduce as in the previous case $m_l < m \leq m_r$, and therefore the constant value of $\pi_1^{(3)}$ implies that all states in the 3-R wave and $\boldsymbol{u}_r$ correspond to the points on $R_3^+(\boldsymbol{v}_l)$ where

$$R_3^+(\boldsymbol{v}_l) = \left\{(m, \theta)/\theta \in \theta^+(m), m_l < m < \infty\right\}, \tag{3.9}$$

i.e., $R_3^+(\boldsymbol{v}_l)$ curve is given by

$$\theta = \theta_l + \int_{m_l}^{m} \sqrt{\frac{-G'}{mG(m)}} dm, \ m_l < m. \tag{3.10}$$

This gives a value of θ such that $\theta > \theta_l$ for $m > m_l$ and the curve $R_3^+(\boldsymbol{v}_l)$ is above the line $\theta = \theta_l$ with $m > m_l$ (Fig. 3.1). Thus, the set of points $R_3^+(\boldsymbol{v}_l)$ which can be connected to a state (m_l, θ_l) on the left by a 3-R wave is a part of the rarefaction curve of the third family, i.e. $R_3(\boldsymbol{v}_l)$.

As $\theta^+(m)$ (and also $-\theta^-(m)$) may tend to infinity, θ on these curves may take numerically any large value. From the point of view of physically realistic situations, we need to consider only the strip $-\pi < \theta - \theta_l < \pi$ in the (m, θ)-plane as shown in Fig. 3.4, though the part $-\pi < \theta - \theta_l < 0$ cannot be attained by a rarefaction wave. At the end of the section 2, we made relevant comments on the limitations of values of θ through a shock transition (which we shall prove later in this section). Taking all transitions, we shall see that the points in the (m, θ)-plane which are of interest to our discussion lie in the strip $-\pi < \theta - \theta_l < \pi$. In Fig. 3.4, T denotes the curve represented by (3.3) with θ_-^* replaced by $\theta_1 = \theta_+^*(\boldsymbol{v}_l)$ which is also the $R_3^+(\boldsymbol{v}_1)$ curve with $\boldsymbol{v}_1 = (1, \theta_1)$.

Fig. 3.4 has been drawn on the assumption that $\theta_+^*(\boldsymbol{v}_l) < \pi$. However it may turn out that $\theta_+^*(\boldsymbol{v}_l) > \pi$. In this case, the figure has to be modified. $R_1^-(\boldsymbol{v}_l)$ would now intersect the

line $\theta = \pi$, the curve T would disappear and we shall get only four domains A, B, C and D where $\boldsymbol{v}_r$ may lie.

Consider now an elementary wave of the second characteristic family in a solution joining two constant states $\boldsymbol{u}_l$ and $\boldsymbol{u}_r$. Since this family is linearly degenerate, the elementary wave solution will be a contact discontinuity moving with the speed zero. Thus, the R-H conditions for the conservation laws (2.1)-(2.3) imply $m_l = m_r$, $\theta_l = \theta_r$ and a discontinuity in g. The set of points C in (m, θ)-plane, which can be joined to a point (m_l, θ_l) by a contact discontinuity, consists only of just one point: the point (m_l, θ_l) itself. At a point P of the contact discontinuity on Ω_t, the slope dy/dx of Ω_t is continuous. This follows from (1.7).

Next we consider two states $\boldsymbol{u}_l$ and $\boldsymbol{u}_r$ which satisfy the jump relations (2.9) and (2.10) with $s \neq 0$. Then the two states are joined by one of two shocks 1-S and 3-S (of first and the third characteristic families respectively) passing through the origin. When we use the expression (3.5) in Lax's stability condition $c_1(\boldsymbol{u}_r) < s < c_1(\boldsymbol{u}_l)$ for 1-S shock, we get

$$\frac{m_l}{m_r} < \frac{G(m_l)(-G'(m_l))}{G(m_r)(-G'(m_r))}. \tag{3.11}$$

As in the case of 1-R wave, we can show that this inequality implies $m_l < m_r$. Since $s \neq 0$, (2.10) and $m_l < m_r$ give

$$g_r = \frac{G(m_r)}{G(m_l)} g_l < g_l. \tag{3.12}$$

From Lax's stability condition, since we have $s < 0$ for 1-S, it follows from (2.11) that $\theta_r < \theta_l$ and from (2.13) that

$$-\frac{\pi}{2} < \theta_r - \theta_l < 0. \tag{3.13}$$

Thus (2.14) for 1-S gives

$$\theta_r - \theta_l = -\cos^{-1}\left(\frac{m_l G(m_l) + m_r G(m_r)}{m_l G(m_r) + m_r G(m_l)}\right) = -h(m_l, m_r), \text{ (say)} \tag{3.14}$$

where we take only the positive determination of the $\cos^{-1}$ function.

We first study the properties of the function $h(m_l, m)$ not only for $m \geq m_l$ but also for $1 < m < m_l$.

Lemma The function

$$f(m_l, m) = \frac{m_l G(m_l) + m G(m)}{m_l G(m) + m G(m_l)} \tag{3.15}$$

has a maximum value 1 at $m = m_l$. It monotinically decreases for $m > m_l$ and tends to zero as $m \to \infty$ and monotonically increases from $1/m_l$ to 1 in $1 < m < m_l$.

Proof: Proof of the Lemma is simple when we note that

$$\frac{df}{dm}(m_l, m) = \frac{(m^2 - m_l^2) G(m_l) G'(m) + m(G^2(m) - G^2(m_l))}{(m G(m_l) + m_l G(m))^2}$$

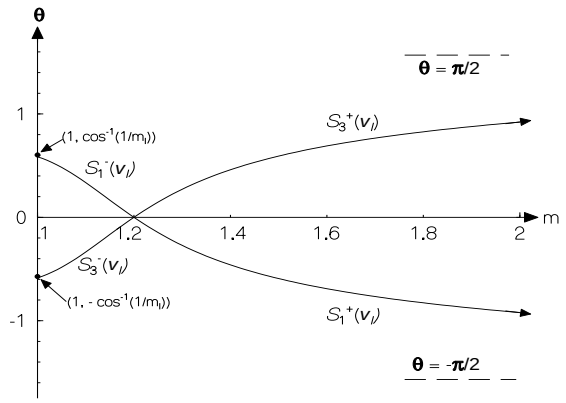

3.2: *Hugoniot curves* $S_1(\boldsymbol{v}_l) = S_1^+(\boldsymbol{v}_l) \cup S_1^-(\boldsymbol{v}_l) \cup \{\boldsymbol{v}_l\}$ *and* $S_3(\boldsymbol{v}_l) = S_3^+(\boldsymbol{v}_l) \cup S_3^-(\boldsymbol{v}_l) \cup \{\boldsymbol{v}_l\}$ *of first and third families with* $m_l = 1.2$, $\theta_l = 0$.

and G and G' satisfy the assumptions **A1-A3** in section 2. ∎

Thus, the curve represented by

$$\theta = \begin{cases} \theta_l + h(m_l, m) & \text{if } 1 < m < m_l \\ \theta_l - h(m_l, m) & \text{if } m > m_l, \end{cases} \tag{3.16}$$

where we take only the positive determination of $\cos^{-1}$, is a curve with continuously turning tangent and is defined in the whole interval $1 < m < \infty$. We denote this curve by $S_1(\boldsymbol{v}_l)$. $\theta - \theta_l$ decreases continuously from $\lim_{m\to 1+}(\theta - \theta_l) = \cos^{-1}(1/m_l)$ to $-\pi/2$ as m varies from 1 to ∞. $S_1(\boldsymbol{v}_l)$ is called Hugoniot curve of the first family.

We denote the upper part of $S_1(\boldsymbol{v}_l)$, given by $\theta = \theta_l + h(m_l, m)$ for $1 < m < m_l$, by $S_1^-(\boldsymbol{v}_l)$. Since for 1-S shock, $m_l < m_r$, the points on this part cannot be reached by 1-S shock from a state $\boldsymbol{u}_l$ on the left. The lower part $S_1^+(\boldsymbol{v}_l)$ given by $\theta = \theta_l - h(m_l, m), m > m_l$ consists of the points $\boldsymbol{v}_r$ which can be joined to $\boldsymbol{v}_l$ by a shock of the first family. The curve $S_1(\boldsymbol{v}_l)$ has been shown in Fig. 3.2 with $\theta_l = 0$.

Consider now a shock of the third characteristic family i.e., 3-S shock, with states $\boldsymbol{u}_l$ on the left and $\boldsymbol{u}_r$ on the right. The Lax's entropy inequality implies $m_l > m_r$. Thus, for 3-S shock, we have

$$m_l > m_r, \quad g_l < g_r, \quad -\cos^{-1}\left(\frac{1}{m_l}\right) < \theta_r - \theta_l < 0. \tag{3.17}$$

The curve $S_3(\boldsymbol{v}_l)$, called as Hugoniot curve of the third family, represented by

$$\theta = \begin{cases} \theta_l - h(m_l, m) & \text{if } 1 < m < m_l \\ \theta_l + h(m_l, m) & \text{if } m > m_l, \end{cases} \tag{3.18}$$

is a reflection of $S_1(\boldsymbol{v}_l)$ in the line $\theta = \theta_l$ as seen in Fig. 3.2 with $\theta_l = 0$. The part

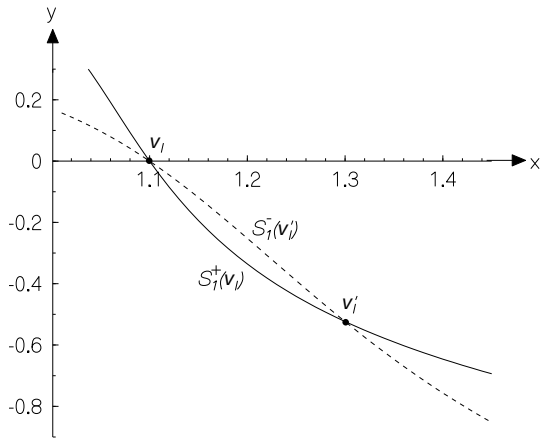

Fig. 3.3: *$S_1^+(\boldsymbol{v}_l)$ and $S_1^-(\boldsymbol{v}_l')$ curves meeting at the points $\boldsymbol{v}_l$ and $\boldsymbol{v}_l'$.*

$S_3^-(\boldsymbol{v}_l)$ of $S_3(\boldsymbol{v}_l)$ represents the set of points which can be joined to $\boldsymbol{u}_l$ by a 3-S shock. Points on the part $S_3^+(\boldsymbol{v}_l)$ cannot be reached from $\boldsymbol{v}_l$ by a 3-S shock.

The following result is an important property which follows immediately from the fact that $h(m_l, m)$ is symmetric with respect to m_l and m.

Lemma If $\boldsymbol{v}_l' = (m_l', \theta_l')$ lies on $S_1^+(\boldsymbol{v}_l)$, then (m_l, θ_l) lies on $S_1^-(\boldsymbol{v}_l')$.

Note that the above curves $S_1^+(\boldsymbol{v}_l)$ and $S_1^-(\boldsymbol{v}_l')$ are two distinct curves meeting at the points $\boldsymbol{v}_l$ and $\boldsymbol{v}_l'$ as shown in Fig. 3.3. In fact, we can make a less precise statement: if $\boldsymbol{v}_l'$ lies on $S_1(\boldsymbol{v}_l)$, then $\boldsymbol{v}_l$ lies on another curve $S_1(\boldsymbol{v}_l')$. This shows that through $\boldsymbol{v}_l$, an infinity of S_1 curves other than $S_1(\boldsymbol{v}_l)$ pass. Similar result is true for S_3 curves. However, the one parameter family of curves $R_i(\boldsymbol{v}_l)$, $i = 1$ or 3 is much simpler. If $\boldsymbol{v}_l'$ lies on $R_i(\boldsymbol{v}_l)$, then $R_i(\boldsymbol{v}_l) = R_i(\boldsymbol{v}_l')$. Through each point $\boldsymbol{v}_l$, only one R_i, $i = 1, 3$ curve passes.

The S_i (i=1,3) curve seems to have a point of inflection. Even for the particular function G given in (2.4), the second derivative of $h(m_l, m)$ is a complicated function. We numerically compute the derivative $\frac{d}{dm}h(m_l, m)$ for various values of k and n and look for its extremum point with respect to m. This will give the point of inflection of S_i. We find that S_i curves have no point of inflection for $k = 1$, $n = 1$. Without a point of inflection, the curve $S_3(\boldsymbol{v}_l)$ is everywhere concave and the curve $S_1(\boldsymbol{v}_l)$ is everywhere convex. For $k = n$ close to 1, the point of inflection is at a point m_f close to 1. As $k = n$ increase, m_f increases and tends to m_l as $k = n \to \infty$, but does not seem to cross m_l.

In this section *we have studied the curves $R_1(\boldsymbol{v}_l)$, $R_3(\boldsymbol{v}_l)$, $S_1(\boldsymbol{v}_l)$, and $S_3(\boldsymbol{v}_l)$, and their different parts such as $R_1^-(\boldsymbol{v}_l)$; passing through any point (m_l, θ_l) in the half plane $m > 1$ when G satisfies the assumptions* **A1**-**A4** *in the section 2.* In spite of the fact that both the

denominator and numerator of $\frac{d}{dm}h(m_l, m)$ vanish simultaneously at $m = m_l$, each one of these curves if not smooth have at least continuously turning tangent.

Dependence of $R_1(\boldsymbol{v}_l)$ (or $R_3(\boldsymbol{v}_l)$) on m_l and θ_l is very simple, as we have described earlier, $R_1(\boldsymbol{v}_l')$ can be obtained from $R_1(\boldsymbol{v}_l)$ by translating $R_1(\boldsymbol{v}_l)$ in θ direction by $\theta_l' - \theta_l + \int_{m_l'}^{m_l} \left\{\frac{-G'(m)}{mG(m)}\right\}^{1/2} dm$. Dependence of $S_1(\boldsymbol{v}_l)$ (or $S_3(\boldsymbol{v}_l)$) on θ_l is also simple: $S_1(\boldsymbol{v}_l, \theta_l)$ can be obtained from $S_1(\boldsymbol{v}_l, \theta_l')$ by translating the later by $\theta_l' - \theta_l$. Even though there are infinity of S_1 passing through $\boldsymbol{v}_l$, $S_1(\boldsymbol{v}_l)$ is unique and different from all other $S_1(\boldsymbol{v}_l')$ which pass through $\boldsymbol{v}_l$. The variation of $S_1(\boldsymbol{v}_l)$ on m_l, when θ_l is kept constant, is also not very complicated. We first note that when m_l decreases, $\theta_l + \cos^{-1}\frac{1}{m_l}$ decreases to θ_l. We use the lemma (3.1) to deduce

$$f(m, m_{l1}) < f(m, m_{l2}) \text{ for } m_{l1} < m_{l2} < m \text{ and } f(m, m_{l1}) > f(m, m_{l2}) \text{ for } m < m_{l1} < m_{l2}$$

so that

$$h(m, m_{l1}) > h(m, m_{l2}) \text{ for } m_{l1} < m_{l2} < m \text{ and } h(m, m_{l1}) < h(m, m_{l2}) \text{ for } m < m_{l1} < m_{l2}.$$

Since h is a symmetric function of its arguments, the above relations lead to $\theta_l - h(m_{l1}, m) < \theta_l - h(m_{l2}, m)$ for $m_{l1} < m_{l2} < m$ and $\theta_l + h(m_{l1}, m) < \theta_l + h(m_{l2}, m)$ for $m < m_{l1} < m_{l2}$.

Thus, the curve $S_1(m_{l1}, \theta_l)$, which varies from $\theta_l + \cos^{-1}\frac{1}{m_{l1}}$ to $-\pi/2$, always lies below the curve $S_1(m_{l2}, \theta_l)$ when $m_{l1} < m_{l2}$. Similarly, it can be shown that $S_3(m_{l1}, \theta_l)$ lies above the curve $S_3(m_{l2}, \theta_l)$ when $m_{l1} < m_{l2}$.

From the properties just discussed, we prove

Theorem 3.1 Two members of either R_1 family or R_3 family or S_1 family or S_3 family do not intersect when only one of the two variable m_l and θ_l varies.

This theorem is important as it helps us in solving the Riemann problem.

The set of points in (m, θ)-plane, which can be connected to $\boldsymbol{v}_l$ (with $\theta_l = 0$) by a shock or a centered rarefaction wave, have been shown in Fig. 3.4. In addition to that, we have also shown in Fig. 3.4 a part T of $R_3^+(m = 1, \theta = \theta_+^*(\boldsymbol{v}_l))$ for $\theta_+^*(\boldsymbol{v}_l) < \theta < \pi$ by a broken curve. The points in (m, θ)-plane relevant to our discussion lie in the domain $1 < m < \infty$, $-\pi < \theta < \pi$. We denote different parts of this domain by A, B, C, D and E as follows:

A: Bounded by $R_1^-(\boldsymbol{v}_l)$, T, $\theta = \pi$ and R_3^+

B: Bounded by $R_3^+(\boldsymbol{v}_l)$, $S_1^+(\boldsymbol{v}_l)$ and $m = \infty$

C: Bounded by $S_3^-(\boldsymbol{v}_l)$, $S_1^+(\boldsymbol{v}_l)$, $\theta = -\pi$ and $m = 1$

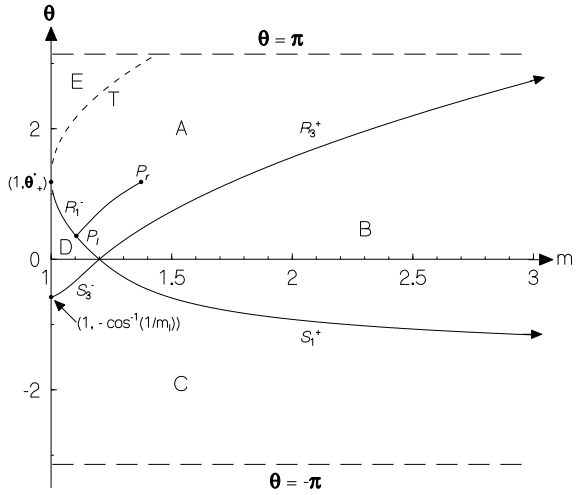

Fig. 3.4: *Rarefaction and Hugoniot curves.*

D: Bounded by $m = 1$, $R_1^-(\boldsymbol{v}_l)$ and $S_3^-(1, \boldsymbol{v}_l)$

E: Bounded by $m = 1$, $\theta = \pi$ and $T(1, \theta_+^*(\boldsymbol{v}_l))$.

It is important to note that if $\theta_+^* \geq \pi$, then the set E is a void set.

4 Geometrical features arising out of the elementary wave solutions: elementary shapes

A Riemann problem for the system of conservation laws (2.1) is to find a weak solution of the system in the upper half plane: $(\xi, t) \in I\!R \times I\!R_+$, satisfying a cauchy data

$$\boldsymbol{u}(x, 0) = \begin{cases} \boldsymbol{u}_l, & \text{if } \xi < 0, \text{ with } \theta_l = 0 \\ \boldsymbol{u}_r, & \text{if } \xi \geq 0, \end{cases} \tag{4.1}$$

where $\boldsymbol{u}_l$ and $\boldsymbol{u}_r$ are two constant states and for this system, we can choose $\theta_l = 0$ without any loss of generality. Since g is the metric along the wavefront Ω_t, the initial position Ω_0 of the front is obtained by integrating the equation (1.7) (see Prasad, 2001, 3.3.10) with g and θ as given in (4.1). Thus $\Omega_0 : (x_0(\xi), y_0(\xi))$ is

$$(x_0(\xi), y_0(\xi)) = \begin{cases} (0, g_l\xi) & , \text{ if } \xi \leq 0 \\ (\xi g_r \sin\theta_r, \xi g_r \cos\theta_r) & , \text{ if } \xi > 0, \end{cases} \tag{4.2}$$

which has a singularity at the origin $(0, 0)$ joining two straight parts. This singular point is not necessarily a kink unless $\boldsymbol{v}_r$ lies either on $S_1^+(\boldsymbol{v}_l)$ or $S_3^-(\boldsymbol{v}_l)$ as discussed in section 3. Once the Riemann problem is solved in the (ξ, t)-plane, the mapping from (ξ, t)-plane to (x, y)-plane is obtained by integrating the ray equations (1.6) for a fixed value of ξ,

$$x(\xi, t) \;\; = \;\; x_0(\xi) + \int_0^t m(\xi, \tau)\cos(\theta(\xi, \tau))d\tau, \tag{4.3}$$

$$y(\xi,t) \;=\; y_0(\xi) + \int_0^t m(\xi,\tau)\sin(\theta(\xi,\tau))d\tau. \tag{4.4}$$

A ray starting from (x_0, y_0) is given by (4.3)-(4.4) when ξ is kept fixed. The wavefront Ω_t at any point is again given by (4.3)-(4.4) when t is kept fixed and ξ varies.

Now we consider the structure of a 1-R wave in (ξ, t)-plane and the geometrical shape $\mathcal{R}_1$, of the wavefront Ω_t associated with this solution. To get a 1-R wave as a solution of the Riemann problem, we choose the state $\boldsymbol{v}_r$ to lie on $R_1^-(\boldsymbol{v}_l)$ curve and $g_l G(\boldsymbol{v}_r) = g_r G(\boldsymbol{v}_l)$.

If $g_l \neq g_r$, there must be a contact discontinuity along $\xi = 0$, hence we first solve m as a function of ξ/t from

$$\frac{mG(m)}{g^2(-G'(m))} = \left(\frac{\xi}{t}\right)^2,\; g = \frac{g_l G(m)}{G(m_l)}; c_1(\boldsymbol{v}_l) < \frac{\xi}{t} \leq c_1(\boldsymbol{v}_r, g_L), \tag{4.5}$$

where

$$g_L = \left.\frac{g_l G(m)}{G(m_l)}\right|_{\xi/t = c_1(\boldsymbol{u}_r)}. \tag{4.6}$$

Since $\frac{m}{-G'}$ is a monotonically increasing function, the solution $m = m(\xi/t)$ exists uniquely. Then the solution is given by (see Fig. 4.1)

$$\boldsymbol{u} \;=\; \boldsymbol{u}_l, \qquad \text{if } -\infty < \xi \leq c_1(\boldsymbol{u}_l)t \tag{4.7}$$

$$\;=\; \begin{cases} m(\xi/t), \\ \theta = \theta_l + \int_m^{m_l} \sqrt{\frac{(-G')}{mG}}dm, \\ g = g_l \frac{G(m)}{G(m_l)}, \end{cases} \quad \text{if } c_1(\boldsymbol{u}_l)t < \xi \leq c_1(\boldsymbol{v}_r, g_L)t \tag{4.8}$$

$$\;=\; \begin{cases} m_r, \\ \theta_r, \\ g = g_L, \end{cases} \quad \text{if } c_1(\boldsymbol{u}_L)t < \xi \leq 0 \tag{4.9}$$

$$\;=\; \boldsymbol{u}_r, \qquad \text{if } 0 < \xi < \infty. \tag{4.10}$$

The 1-R solution is completely determined. Fig. 4.2 shows the geometry of the wavefront Ω_t associated with this solution. The wavefront Ω_t contains a curved part $\mathcal{R}_1$ of the wavefront, which we call an *elementary shape* $\mathcal{R}_1$. Ω_t and rays can be determined with the help of (4.3)-(4.4) as explained there. The rays starting from the points below the singularity at $\xi = 0$ on Ω_0 enter $\mathcal{R}_1$ zone in the (x, y)-plane from below, curve upward and finally emerge out of this zone again as straight lines. Thus the elementary shape $\mathcal{R}_1$ propagates downwards on Ω_t.

As in the case of $\mathcal{R}_1$ above, *we define an elementary shape on Ω_t to be the image in (x, y)-plane of an elementary wave solution of the system of conservation laws.* We denote these elementary shapes by $\mathcal{R}_1$, $\mathcal{R}_3$, $\mathcal{C}$, $\mathcal{K}_1$, and $\mathcal{K}_3$ where $\mathcal{R}_3$ corresponds to 3-R wave, $\mathcal{C}$

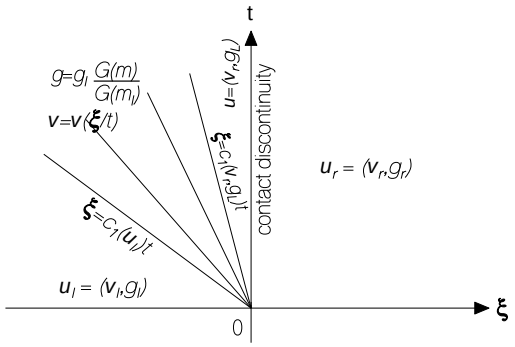

Fig. 4.1: *Solution of the Riemann problm when* $\boldsymbol{v}_r \in R_1^-(\boldsymbol{v}_l)$.

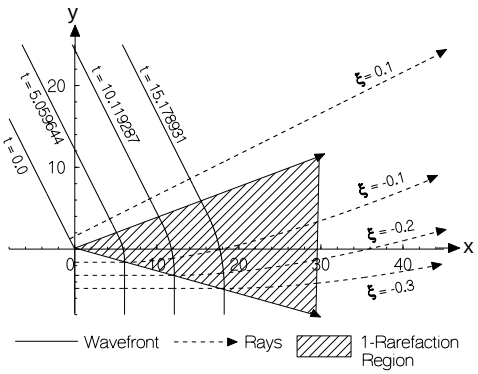

Fig. 4.2: $\mathcal{R}_1$ *elementary shape with* $m_l = 1.2$, $m_r = 1.08$ *and* θ_r*=0.4649.*

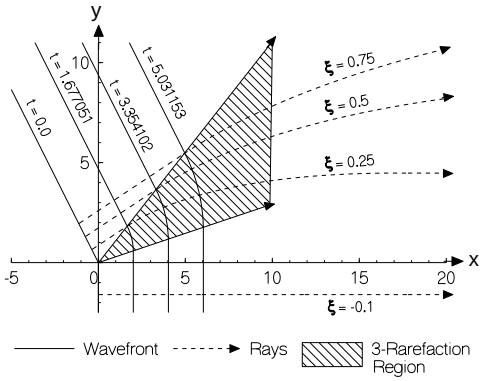

Fig. 4.3: $\mathcal{R}_3$ *elementary shape with* $m_l = 1.2$, $m_r = 1.4$ *and* θ_r*=0.5239.*

to a contact discontinuity, $\mathcal{K}_1$ to a 1-S shock and $\mathcal{K}_3$ to a 3-S shock. Note that $\mathcal{C}$, $\mathcal{K}_1$ and $\mathcal{K}_3$ are point singularities on Ω_t.

As the case of 1-R solution, we can discuss the structure of 3-R centered wave and the associated elementary shape $\mathcal{R}_3$. They have been shown in Fig. 4.3. $\mathcal{R}_3$ is also convex, but unlike $\mathcal{R}_1$, the elementary shape $\mathcal{R}_3$ moves upwards on Ω_t and the rays starting from the points on the upper part of Ω_0, enter $\mathcal{R}_3$ zone from above and finally emerge out of this zone as straight lines.

It is easy to derive the boundary lines of a $\mathcal{R}_1$ zone (or $\mathcal{R}_3$ zone) in the (x, y)-plane. Let us do this for the $\mathcal{R}_1$ zone. The two characteristic lines which bound the 1-R wave in the (ξ, t)-plane are $\xi = c_1(\boldsymbol{u}_l)t$, and $\xi = c_1(\boldsymbol{u}_r)t$ (see Fig. 4.1). Since the lower part of Ω_0 is the lower half of the y-axis, a point on the image of $\xi = c_1(\boldsymbol{u}_l)t$ can be reached by a ray starting from $(0, g_l\xi)$, $\xi < 0$ and moving with the velocity m_l in x-direction. Hence, the equation of the lower boundary of the image of (4.8) in (x, y)-plane is given parametrically in terms of

t as

$$x = m_l t,\ y = g_l \xi = g_l c_1(\boldsymbol{u}_l) t \tag{4.11}$$

or since

$$\frac{g_l c_1(\boldsymbol{u}_l)}{m_l} \ = \ -\sqrt{\frac{G(m_l)}{m_l(-G'(m_l))}},$$

this lower boundary of R_1-zone obtained by eliminating t from (4.1), is

$$y = -x\sqrt{\frac{G(m_l)}{m_l(-G'(m_l)}}. \tag{4.12}$$

To get the image of $\xi = c_1(\boldsymbol{v}_r, g_L)t$, i.e., the upper boundary of $\mathcal{R}_1$-zone, we refer to the Fig. 4.1 in (ξ, t)-plane, which is pre-image of Fig. 4.2. A point $(c_1(\boldsymbol{v}_r, g_L)t, t)$ in Fig. 4.1, can be reached from the origin first moving vertically up along the t-axis and then moving horizontally in negative ξ direction. Thus a point on the upper boundary of 1-R region in (x, y)-plane can be reached from the origin by moving along the ray with velocity $(m_r \cos\theta_r, m_r \sin\theta_r)$ and then moving along the wavefront Ω_t. The second movement correspond to a displacement $(-g_L\xi \sin\theta_r, g_L\xi \cos\theta_r)$ in the Fig. 4.2 from the point $(m_r t \cos\theta_r, m_r t \sin\theta_r)$. Therefore, the image of $\xi = c_1(\boldsymbol{v}_r, g_L)t$ is given by

$$x = -g_L\xi \sin\theta_r + m_r t \cos\theta_r, y = -g_L\xi \cos\theta_r + m_r t \sin\theta \tag{4.13}$$

or using $\xi = c_1(\mathbf{v}_r, g_L)t$, we write it as

$$y = \left(\frac{g_L c_1(\boldsymbol{v}_r, g_L)\cos\theta_r + m_r \sin\theta_r}{-g_L c_1(\boldsymbol{v}_r, g_L)\sin\theta_r + m_r \cos\theta_r}\right) x. \tag{4.14}$$

We note that the lower boundary of $\mathcal{R}_1$-zone always has a negative slope, the upper boundary may slope upward, for example for $0 < \theta_r < \pi/2$, if

$$\frac{g_r}{g_L}\sqrt{\frac{m_r(-G'(m_r))}{G(m_r)}} < \cot\theta_r, \tag{4.15}$$

where g_L is given by (4.6).

Consider now a solution $\boldsymbol{u}$ with constant $\boldsymbol{v} = (m_l, \theta = 0)$ in the whole of (ξ, t)-plane and a contact discontinuity along $\xi = 0$ across which $[g] \neq 0$. Since m on Ω_t is constant equal to m_l and $\theta = 0$, the wavefront Ω_t is a straight line $x = m_l t$ parallel to y-axis and the elementary shape $\mathcal{C}$ corresponding the contact discontinuity consists of a single point on the ray $\xi = 0$ i.e., $y = 0$. This elementary shape is not observable on the wavefront. However, if a contact discontinuity appears in a solution in which Ω_t is not a straight line and g is not constant on Ω_t (with a jump on $\mathcal{C}$), then the second derivatives, $x_{\xi\xi}$ and $y_{\xi\xi}$, obtained

from (1.7) show that though the tangent direction of Ω_t is continuous, its curvature may be discontinuous across $\mathcal{C}$.

When the Riemann data (4.1) is such that $(m_r, \theta_r) \in S_1^+(\boldsymbol{v}_l)$, and (3.12) is satisfied, the solution contains only one elementary wave solution, namely 1-S shock. The shock starts from the origin in (ξ, t)-plane and moves with a negative velocity (2.11), since $\theta_r < 0$. The image of the 1-S shock in (ξ, t)-plane is a $\mathcal{K}_1$-kink in (x, y)-plane, its path i.e., the kink path is

$$y = x\left(\frac{m_r - m_l\cos\theta_r}{m_l\sin\theta_r}\right) \tag{4.16}$$

(see the expression (3.3.33) for the kink slope S in Prasad, 2001). A ray starting from the lower part of Ω_0 (i.e., with $\xi_0 < 0$) moves parallel to the x-axis, intersects the kink path and then changes its direction so as to make an angle $\theta_r < 0$ with the x-axis (Fig. 4.4).

Similarly, we can consider a Riemann data which leads to the elementary wave 3-S. The image of this shock is an elementary shape $\mathcal{K}_3$-kink. The geometry of the wavefront Ω_t, rays and the kink path corresponding to this solution has been shown in Fig. 4.5.

Suppose now that the state $\boldsymbol{u}_r$ be such that (m_r, θ_r) lies either on R_1^-, or R_3^+ or S_1^+ or S_3^- but without satisfying the relation (3.5), then the solution of the Riemann problem consists of either a 1-R wave or a 3-R wave or 1-S wave or 3-S wave respectively and in addition there will be a contact discontinuity on $\xi = 0$. When (m_r, θ_r) lies on $R_3^+(\boldsymbol{v}_l)$, the contact discontinuity will on the left of 3-R wave and when (m_r, θ_r) lies on $S_1^+(\boldsymbol{v}_l)$ the contact discontinuity will be on the right of 1-S shock and so on.

The solution of the Riemann problem when (m_r, θ_r) is an arbitrary point in (m, θ)-plane, have been presented in the next section. Here we first analyze whether we can take $g/G(m)$ to be the same constant on the two sides of a 1-S or 3-S shock. This question was raised by Whitham in his heuristic theory of shock dynamics. The answer to the question follows immediately from the jump relation (2.10) with $s \neq 0$. Hence across both shocks, $g/G(m)$ has the same value and in a smooth solution $g/G(m)$ =constant is an integral of the conservation law (1.3). Thus, it is possible to take $g/G(m)$ to be the same constant in the solution in (ξ, t)-plane on the two sides of a shock.

Next, we analyze whether we can replace the system of three conservation laws (1.1)-(1.3) simply by a system of two conservation laws (1.1)-(1.2) with a given expression for $g = G(m)$, as done in a previous work (Prasad and Sangeeta, 1999) for solutions which are continuous (except for shocks) but piecewise smooth in (ξ, t)-plane. We consider an initial value for the system of conservation laws (1.1)-(1.3):

$$\boldsymbol{u}(\xi, 0) = \boldsymbol{u}_0(\xi) \tag{4.17}$$

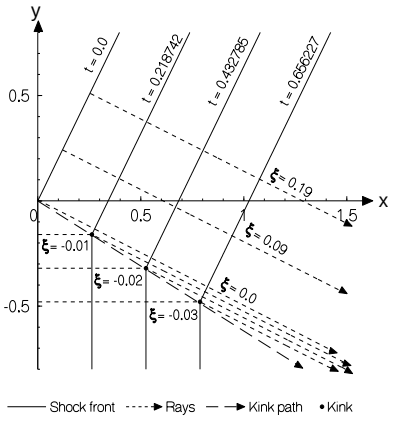

Fig. 4.4: $\mathcal{K}_1$ *with* $m_l = 1.2$, $m_r = 1.4$ and θ_r = -0.46.

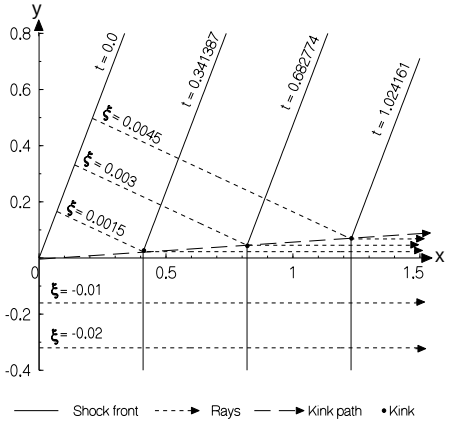

Fig. 4.5: $\mathcal{K}_3$ *with* $m_l = 1.2$, $m_r = 1.08$ and θ_r = -0.3989.

such that

$$g_0(\xi) = G(m_0(\xi)). \tag{4.18}$$

We can always achieve (4.18) in an initial data by replacing ξ by a new function of ξ (Prasad, 2001, page 209). For a smooth solution, we can integrate the equation (1.3) (with $C = m$) to get $g/G(m)$ as a function of ξ which is identically equal to 1, since $g_0/G(m_0) = 1$ from (4.18). Hence

$$g(\xi, t) = G(m(\xi, t)). \tag{4.19}$$

If the solution $\boldsymbol{u}(\xi, t)$ is continuous but piecewise smooth due to presence of simple waves or more complex solutions in some sub-domains of $\mathbb{R}\times\mathbb{R}_+$, then across the common boundaries of smooth regions, the relation (4.19) remains valid. When 1-S and 3-S shocks appear in the solution, $g_l/G(m_l) = g_r/G(m_r)$ being the common jump relation for both shocks, we find that g/G remains continuous across these shock paths. Thus we note that a constant value of $g/G(m)$ is carried along lines ξ= constant as t evolves as long as the solution is continuous and when there is a shock, the same value of g/G crosses over the shock and is again maintained afterward along ξ = constant lines. Thus (4.18) implies (4.19) in all continuous (except for shocks) and piecewise smooth solutions. This justifies the use of the relation (4.19) and the KCL (1.1)-(1.2), provided we choose the initial data satisfying (4.18) as done by Prasad and Sangeeta (1999). With such a choice of ξ, since m is continuous across a contact discontinuity, g is also continuous across it i.e., the contact discontinuity disappears. For a Riemann initial data (4.1), this would mean a suitable choice of ξ i.e., a choice of g on the two sides of $\xi = 0$ such that $g_l/G(m_l) = g_r/G(m_r) = 1$. Thus we have justified the use of the relation (4.19) along with the KCL (1.1)-(1.2) to discuss the propagation of a nonlinear wavefront even for the initial data (4.1) which is discontinuous at a number of isolated points on ξ-axis but otherwise smooth. However, though contact discontinuities disappear, their trace on Ω_t may still be seen as a discontinuity in the curvature of Ω_t. But a discontinuity in

the curvature of Ω_t may exist even in a piecewise C^1 solution of (1.1) and (1.2) with (4.19) due to discontinuity in the derivatives of m, for example across a curve in (ξ, t)-plane which forms the boundary of a simple wave.

5 Geometrical shapes arising out of a general singularity on Ω_t

In this and the next section, we shall use the relation (4.19) instead of the conservation law (1.3). Our governing equations are then the KCL (1.1)-(1.2) with (4.19). We shall first study the general Riemann problem, when the point $\boldsymbol{v}_l = (m_l, \theta_l = 0)$ is given and $\boldsymbol{v}_r = (m_r, \theta_r)$ is an arbitrary point in (m, θ)-plane. This problem can be easily solved with the help of the Fig. 3.4 (or a slightly modified figure when $\theta_+^* > \pi$ as mentioned in the section 3).

Let $P_r(m_r, \theta_r)$ be a point in the domain A. The solution of the Riemann problem exists because $R_3^-(\boldsymbol{v}_r)$ being below T, it always meets $R_1^-(\boldsymbol{v}_l)$ and in this case it consists of the state $(m_l, 0)$ on the left of a 1-R wave continuing upto an intermediate constant state $P_i(m_i, \theta_i)$, which ends into a 3-R wave to the right of which we get the final state (m_r, θ_r). This intermediate state (m_i, θ_i) is the point of intersection P_i of the curves $R_1^-(\boldsymbol{v}_l)$ and $R_3^-(\boldsymbol{v}_r)$ which is unique because of the geometry of these curves (see Fig. 3.3) as discussed in section 3. Existence of the unique point of intersection can also be proved by using fixed point method, but it appears that it is unnecessary because of very clear geometrical arguments. It is important to note that, since $R_3(\boldsymbol{v})$ for $\boldsymbol{v} \neq \boldsymbol{v}_l$ is just a translation of $R_3(\boldsymbol{v}_l)$ in θ direction, $R_3^-(\boldsymbol{v}_r)$ can never intersect $R_3^+(\boldsymbol{v}_l)$. This argument ensures the existence of the intermediate point $P_i(m_i, \theta_i)$ as the point of intersection of the $R_1^-(\boldsymbol{v}_l)$ and $R_3^-(\boldsymbol{v}_r)$ curves if $(m_r\theta_r) \in A$. The above argument is equivalent to saying that there exists a unique point $P_i(m_i, \theta_i)$ on the $R_1^-(\boldsymbol{v}_l)$ curve such that $R_3^+(\boldsymbol{v}_i)$ passes through P_r. The shape of the wavefront at $t = 0$ and at times $t > 0$ is shown in Fig. 5.1.

If we have considered the conservation law (1.3) instead of the relation (4.19), we would have got a contact discontinuity along $\xi = 0$ but this would not have affected Fig. 5.1. We describe these result symbolically as

$$(m_r, \theta_r) \in A \rightarrow \mathcal{R}_1\mathcal{R}_3, \tag{5.1}$$

which means that when (m_r, θ_r) is in the domain A, the resultant wavefront has an elementary shape $\mathcal{R}_1$ propagating below on Ω_t, and $\mathcal{R}_3$ propagating above and these two are separated by a plane (straight) section of the front.

Similarly, we get the results

$$(m_r, \theta_r) \in B \rightarrow \mathcal{K}_1\mathcal{R}_3, \tag{5.2}$$

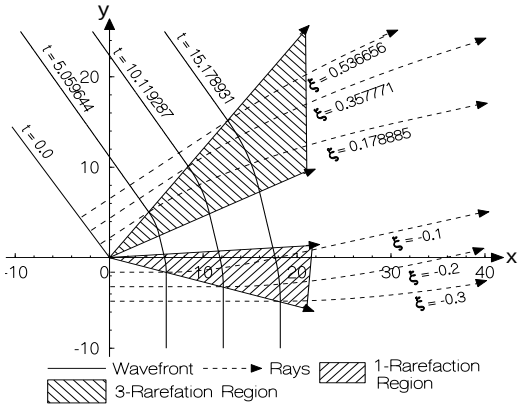

Fig. 5.1: *Geometrical shape of* Ω_t *when* $\boldsymbol{v}_r \in A$ *with* $m_l = 1.2$, $m_r = 1.25$ *and* θ_r=0.6.

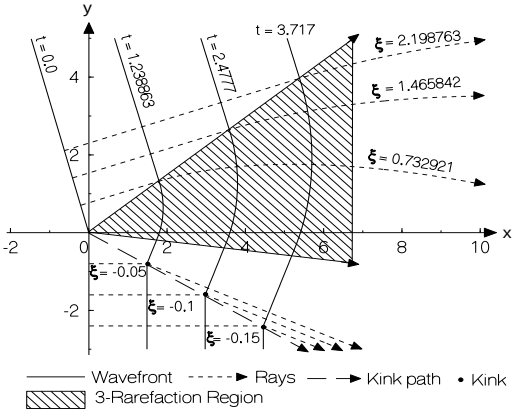

Fig. 5.2: *Geometrical shape of* Ω_t *when* $\boldsymbol{v}_r \in D$ *with* $m_l = 1.2$, $m_r = 1.7$ *and* θ_r=0.35.

and the geometrical shape of the wavefront at different times is shown in Fig. 5.2.

Let $\boldsymbol{v}_r = (m_r, \theta_r) \in C$. We expect the result $\boldsymbol{v}_r \in C \rightarrow \mathcal{K}_1\mathcal{K}_3$ but we face a difficulty now. When the point $\boldsymbol{v}_r$ is close to the curve $S_3^-(\boldsymbol{v}_l)$, then the curve $S_3^+(\boldsymbol{v}_r)$ enters into the domain D. Therefore, it looks as if the curve $S_3^+(\boldsymbol{v}_r)$ may intersect the curve $R_1^-(\boldsymbol{v}_l)$ instead of $S_1^+(\boldsymbol{v}_l)$. But this does not happen. Consider a point $P_r'(m_r, \theta_r')$ on $S_3^-(\boldsymbol{v}_l)$ above the point $P_r(m_r, \theta_r)$. By lemma 3.2, the curve $S_3^+(m_r, \theta_r')$ passes through $\boldsymbol{v}_l = (m_l, 0)$. But the curve $S_3^+(m_r, \theta_r)$ is obtained by translating the curve $S_3^+(m_r, \theta_r')$ in the negative direction of θ-axis by a distance $\theta_r - \theta_r'$ and hence will meet $S_1^+(\boldsymbol{v}_l)$ at a point $P_i(m_i, \theta_i)$. Thus, we get the following result

$$(m_r, \theta_r) \in C \rightarrow \mathcal{K}_1\mathcal{K}_3. \tag{5.3}$$

The geometrical shape of Ω_t if $(m_r, \theta_r) \in C$ is shown in Fig. 5.3.

Similar arguments as above can be made to show the result depicted in Fig. 5.4. i.e.,

$$(m_r, \theta_r) \in D \rightarrow \mathcal{R}_1\mathcal{K}_3. \tag{5.4}$$

Finally, let $(m_r, \theta_r) \in E$. Then $\theta_r > \theta_+^* + \int_1^{m_r} \sqrt{\frac{-G'(m)}{mG(m)}}\, dm$, where θ_+^* is given by (3.2), and hence $R_3^-(\boldsymbol{v}_r)$ touches the line $m = 1$ at $\theta > \theta_+^*$. This shows that there exist no intermediate state which joins $\boldsymbol{u}_l$ on the left and $\boldsymbol{u}_r$ on the right. Thus we get the following theorem.

Theorem 5.1 When $P_r \in E$, there is no solution of the Riemann problem. For every pair m_l and m_r, and m_r sufficiently close to 1; there exists an angle $\theta_c(m_l, m_r)(0 < \theta_c < \pi)$ such that if $\theta_r > \theta_c(m_l, m_r)$, the solution fails to exist.

We have not examined so far in this paper the case $m \rightarrow 1+$. We notice from the

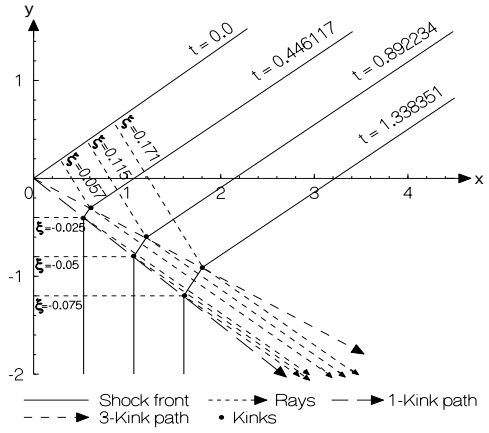

Fig. 5.3: *Geometrical shape of* Ω_t *when* $\boldsymbol{v}_r \in C$ *with* $m_l = 1.2$, $m_r = 1.3$ *and* θ_r=-0.785.

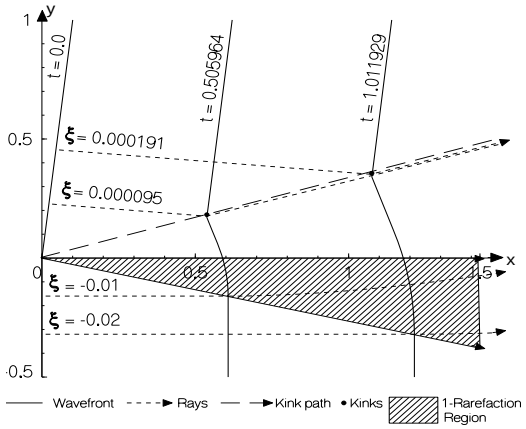

Fig. 5.4: *Geometrical shape of* Ω_t *when* $\boldsymbol{v}_r \in B$ *with* $m_l = 1.2$, $m_r = 1.02$ *and* θ_r=0.35.

from the assumption **A1** in section 2, that $G(m) \to \infty$ as $m \to 1+$. As $gd\xi = G(m)d\xi$ represents an element of length dl along the wavefront Ω_t it follows that between two given rays corresponding to ξ and $\xi + \delta\xi$, the distance $\delta l = G(m)(\delta\xi)$ tends to infinity as $m \to 1+$. It means that the energy flux $F(m) = 1/G(m)$ along a ray tends to zero as $m \to 1+$. The situation is similar to that encountered in gas dynamics where the mass density $\rho \to 0$ implies appearance of a vacuum (Courant and Friedrichs, 1948) in a piston problem when the piston is withdrawn sufficiently rapidly giving a complete simple wave (see also Prasad, 2001, section 3.1.1). In our theory, a *vacuum* with vanishing energy flux appears on the wavefront Ω_t wherever $m \to 1+$.

We have not studied the way in which this limiting process takes place but we can quickly write down the consequences of KCL in the degenerate case when $m = 1$:

$$\theta_t = 0 \quad , \quad g_t = \theta_\xi. \tag{5.5}$$

The first equation states that the rays are straight lines given by $x_t = \cos\theta, y_t = \sin\theta$. The second one is the usual relation of the convergence of rays with the ray tube area. Thus $m = 1$ corresponds to the linear theory. It is an important and difficult problem to study mathematically, the experimentally observed transition from linear to weakly nonlinear results (Sturtevant and Kulkarni (1976)).

6 Interaction of elementary shapes

Elementary shapes on a nonlinear wavefront Ω_t propagate on the front. Two elementary shapes, separated by a straight portion of Ω_t, may or may not interact. The process of

interaction if it takes place, may take finite or infinite time depending on the relative strengths of the two elementary shapes. Although, it is not possible to compute the shape of Ω_t during the process of interaction without a full numerical solution of the conservation laws (1.1)-(1.2), we shall see that we can make a very good prediction of the final results qualitatively. When the interaction period is finite, we show that the final results will again consists of a pair of *elementary shapes*. All these geometrical features of Ω_t can be studied from the corresponding results on the interaction of simple waves and shock waves in (ξ, t)-plane (for Euler's equations of one-dimensional unsteady gas flow, see Courant and Friedrichs (1948), Smoller (1983)).

We have highlighted "elementary shapes" in the last paragraph in italics, since interaction of two elementary waves need not result in waves both of which are elementary because if any one of the two end products is a simple wave, it will not in general be centered. We note that a more general non-centered simple wave in the form of a *compression* wave, in which the characteristics converge in t-increasing direction does not seem to appear after interaction. This conjecture is based on the analysis of all possible interactions. Thus, the resulting waves from a complete interaction of two elementary waves or the reflected wave during the process of reflection is always either a shock wave or a rarefaction wave. Even if this rarefaction (say of ith family) wave is not centered, the Riemann invariants $\left\{\pi_1^{(i)}, \pi_2^{(i)}\right\}$, $i = 1, 3$ are constant. Hence the states $\boldsymbol{v}_r$, which can be joined to a state $\boldsymbol{v}_l$ through a non-centered rarefaction wave, lie on the curve $R_1^-(\boldsymbol{v}_l)$ and $R_3^+(\boldsymbol{v}_l)$. Therefore, we can study interaction of two elementary waves or elementary shapes with the help of Fig. 3.4. For this purpose, we use not the full set of three conservation laws (2.1) but the reduced set of two equations (1.1)-(1.2) with (4.19).

Two elementary shapes on Ω_t separated by a straight part of Ω_t correspond to the initial stages of the solution from the following initial data for (1.1)-(1.2) and (4.19)

$$\boldsymbol{v}(\xi, 0) = \begin{cases} \boldsymbol{v}_l = (m_l, 0) & , \quad -\infty < \xi \leq \xi_l \\ \boldsymbol{v}_0 = (m_0, \theta_0) & , \quad \xi_l < \xi \leq \xi_r \\ \boldsymbol{v}_r = (m_r, \theta_r) & , \quad \xi_r < \xi \leq \infty \end{cases} \tag{6.1}$$

with an appropriate choice of $\boldsymbol{v}_0$ and $\boldsymbol{v}_r$ in terms of $\boldsymbol{v}_l$ and arbitrary $\xi_l, \xi_r \in I\!R$.

In order to describe the result of interaction, we use a notation $\mathcal{E}_i\mathcal{E}_j$ to denote a state of Ω_t corresponding to an elementary shape $\mathcal{E}_i$ joining states $\boldsymbol{v}_l$, $\boldsymbol{v}_0$ and $\mathcal{E}_j$ joining $\boldsymbol{v}_0$ and $\boldsymbol{v}_r$ on Ω_t. Thus $\mathcal{R}_1\mathcal{K}_1 \rightarrow \mathcal{K}_1\mathcal{R}_3$ means that interaction of $\mathcal{R}_1$ elementary shape and $\mathcal{K}_1$ elementary shape will give $\mathcal{K}_1$ kink and $\mathcal{R}_3$ shape. We take up now discussion of all possible interactions: $\mathcal{K}_1\mathcal{K}_1$, $\mathcal{K}_3\mathcal{K}_3$, $\mathcal{R}_1\mathcal{K}_1$, $\mathcal{R}_3\mathcal{K}_3$, $\mathcal{K}_1\mathcal{R}_1$, $\mathcal{K}_3\mathcal{R}_3$, $\mathcal{R}_3\mathcal{R}_1$, $\mathcal{R}_3\mathcal{K}_1$, $\mathcal{K}_3\mathcal{R}_1$ and $\mathcal{K}_3\mathcal{K}_1$ one by one starting first with six simpler cases $\mathcal{R}_3\mathcal{R}_1$, $\mathcal{R}_3\mathcal{K}_1$, $\mathcal{K}_3\mathcal{K}_1$, $\mathcal{K}_3\mathcal{R}_1$, $\mathcal{K}_1\mathcal{K}_1$ and $\mathcal{K}_3\mathcal{K}_3$ where the interactions are always completed in finite time.

(i) $\mathcal{K}_3\mathcal{R}_1$ **interaction:** Here $\boldsymbol{v}_0 \in S_3^-(\boldsymbol{v}_l)$ and $\boldsymbol{v}_r \in R_1^-(\boldsymbol{v}_0)$ so that $\boldsymbol{v}_r \in D$. This is one of the simplest cases but care must be taken such that $m_r > 1$. The result is

$$\mathcal{K}_3\mathcal{R}_1 \to \mathcal{R}_1\mathcal{K}_3. \tag{6.2}$$

(ii) $\mathcal{R}_3\mathcal{K}_1$ **interaction:** Here $\boldsymbol{v}_0 \in R_3^+(\boldsymbol{v}_l)$ and $\boldsymbol{v}_r \in S_1^+(\boldsymbol{v}_0)$ respectively. Since $S_1^+(\boldsymbol{v}_0)$ and $S_1^+(\boldsymbol{v}_l)$ are asymptotic to $\theta = \theta_0 - \pi/2$ and $\theta = \theta_l - \pi/2$ respectively and $\theta_0 > \theta_l$, we have $\boldsymbol{v}_r \in B$ (the proof of this statement is not rigorous but has been verified numerically (see (v) below)). Hence, it follows that

$$\mathcal{R}_3\mathcal{K}_1 \to \mathcal{K}_1\mathcal{R}_3. \tag{6.3}$$

(iii) $\mathcal{K}_3\mathcal{K}_1$ **interaction:** Here $\boldsymbol{v}_0 \in S_3^-(\boldsymbol{v}_l)$ and $\boldsymbol{v}_r \in S_1^+(\boldsymbol{v}_0)$ so that $\boldsymbol{v}_r \in C$. From (5.3) we get

$$\mathcal{K}_3\mathcal{K}_1 \to \mathcal{K}_1\mathcal{K}_3. \tag{6.4}$$

Proof of this statement is also not rigorous because we have not proved that when $\boldsymbol{v}_0$ is very close to $\boldsymbol{v}_l, S_1^+(\boldsymbol{v}_0)$ will not intersect $S_1^+(\boldsymbol{v}_l)$. This has been only numerically verified.

(iv) $\mathcal{R}_3\mathcal{R}_1$ **interaction:** Here $\boldsymbol{v}_0 \in R_3^+(\boldsymbol{u}_l)$ and $\boldsymbol{v}_r \in R_1^-(\boldsymbol{u}_0)$. This interaction will always be complete since the trailing end of 3-R wave has a positive velocity in (ξ, t)- plane and that of 1-R wave has a negative velocity. Since $m_0 > m_l$, $R_1^-(\boldsymbol{v}_0)$ may intersects either the curve T or the boundary $\theta = \pi$. Hence there exists a $\delta_4(m_l, m_0)$ such that for

$$m_0 - m_r = \delta_4(m_l, m_0),\ \boldsymbol{v}_r \in T \text{ or the line } \theta = \pi. \tag{6.5}$$

We give an equation to determine $\delta_4(m_l, m_0)$ in the appendix. Equations for $\delta_i(m_l, m_0)$, i = 7, 8, 9, 10 (which appear below) can be similarly obtained. This leads to the following result

(a) If $m_0 - m_r < \delta_4(m_l, m_0)$, $\boldsymbol{v}_r \in A$ and we have

$$\mathcal{R}_3\mathcal{R}_1 \to \mathcal{R}_1\mathcal{R}_3. \tag{6.6}$$

(b) When $m_0 - m_r = \delta_4$ and $\boldsymbol{v}_r \in T$, the 1-R wave ends up at the point $\boldsymbol{v}_r$ on T - this point can be joined to $\boldsymbol{v}_l$ by a 1-R wave on the left and a 3-R wave on the right through the point $(m = 1,\ \theta = \theta_+^*)$, which represents a vacuum with vanishing energy flux. This is not an acceptable solution as the ray coordinate formulation breaks down. Our theory does not provide any information on the result of this interaction.

(c) when $m_0 - m_r > \delta_4$, and the point $\boldsymbol{v}_r \in E$ and our theory provides no information on the result of this interaction.

(d) When $\boldsymbol{v}_r$ lies on the line $\theta = \pi$, we get a limiting case of the wavefront folding on itself. This degenerate case does not seem to be physically realistic.

(v) $\mathcal{K}_1\mathcal{K}_1$ **interaction:** Here $\boldsymbol{v}_0 \in S_1^+(\boldsymbol{v}_l)$ and $\boldsymbol{v}_r \in S_1^+(\boldsymbol{v}_0)$. It is one of the difficult cases where we are unable to prove whether $S_1^+(\boldsymbol{v}_0)$ which starts from $\boldsymbol{v}_0$, enters into the domain C or the domain B. We take help of drawing the curves $S_1^+(\boldsymbol{v}_0)$ by numerical computation for a large number of values of the parameters k and n in (2.4) and m_0, and verify that the point $\boldsymbol{v}_r$ remains entirely in C. This result as $m \to \infty$ is true, as can be seen from the fact that θ on $S_1^+(\boldsymbol{v}_l)$ tends to $-\pi/2$ and θ on $S_1^+(\boldsymbol{v}_0)$ tends to $\theta_0 - \pi/2$ with $\theta_0 < 0$. Once we accept that $S_1^+(\boldsymbol{v}_0)$ lies entirely in C, we get the result

$$\mathcal{K}_1\mathcal{K}_1 \to \mathcal{K}_1\mathcal{K}_3. \tag{6.7}$$

(vi) $\mathcal{K}_3\mathcal{K}_3$ **interaction:** Situation is similar to the previous case, we do numerical experiments with a large number of cases with the function (2.4) to accept the result that $\boldsymbol{v}_r \in C$ so that

$$\mathcal{K}_3\mathcal{K}_3 \to \mathcal{K}_1\mathcal{K}_3. \tag{6.8}$$

(vii) $\mathcal{R}_1\mathcal{K}_1$ **interaction:** Here $\boldsymbol{v}_0 \in R_1^-(\boldsymbol{v}_l)$ and $\boldsymbol{v}_r \in S_1^+(\boldsymbol{v}_0)$ This is a case when the interaction is not completed in finite time when the strength of the 1-R wave is large compared with that of 1-S wave (we denote it by saying that $\mathcal{R}_1$ is strong compared to $\mathcal{K}_1$). This follows from the theorem on the persistence of a shock (Prasad, 2001, p 35, see also Prasad, 1993)), $\mathcal{K}_1$ cannot disappear in finite time. From numerical computation, we find $S_1^+(\boldsymbol{v}_0)$ to be above $R_1^-(\boldsymbol{v}_l)$ i.e., in the domain A for small values of $m_r - m_0$. Now there exists a value $\delta_7(m_l, m_0)$ say, such that for $m_r - m_0 = \delta_7(m_l, m_0)$, the point $\boldsymbol{v}_r \in R_3^+(\boldsymbol{v}_l)$.

(a) When $m_r - m_0 = \delta_7(m_l, m_0)$, the interaction is completed in infinite time and we get $\lim_{t\to\infty} \mathcal{R}_1\mathcal{K}_1 \to \mathcal{R}_3$. In this case both, 1-R wave and 1-S shock keep on interacting with diminishing strengths and the precise result is

$$\mathcal{R}_1\mathcal{K}_1 \to \mathcal{R}_1\mathcal{K}_1\mathcal{R}_3, \quad \lim_{t\to\infty} \mathcal{R}_1\mathcal{K}_1\mathcal{R}_3 = \mathcal{R}_3. \tag{6.9}$$

In (ξ, t)-plane, the state at any time t on the right side of 1-S shock will also be the state on the left of the 3-R wave and this state will tend to $\boldsymbol{v}_l$ as $t \to \infty$. This is a very interesting case, when two waves of the first family interact and give rise only to a wave of the third family after the interaction. At any finite time we have a shape represented by $\mathcal{R}_1\mathcal{K}_1\mathcal{R}_3$.

(b) When $m_r - m_0 < \delta_7$, $\boldsymbol{v}_r \in A$ and we may think that $\mathcal{R}_1\mathcal{K}_1 \to \mathcal{R}_1\mathcal{R}_3$, which is not strictly correct. The theorem on the persistence of a shock implies that the 1-S shock cannot disappear to form a 1-R wave. The correct result at any finite time t is $\mathcal{R}_1\mathcal{K}_1 \to \mathcal{R}_1\mathcal{K}_1\mathcal{R}_3$. In (ξ, t)-plane, the 1-R wave on the left continues to interact indefinitely with the 1-S shock

(the shock is unable to penetrate the 1-R wave fully), then appears asymptotically a constant state $\boldsymbol{v}_i$ which is the state behind the 1-S shock and into which the 3-R wave ends on its left. The strength of 1-S shock tends to zero but the two expansion waves 1-R and 3-R will have finite strength confirming

$$\lim_{t\to\infty} \mathcal{R}_1\mathcal{K}_1\mathcal{R}_3 = \mathcal{R}_1\mathcal{R}_3$$

a result which we get from the fact that $\boldsymbol{v}_r \in A$. Thus, we get

$$\mathcal{R}_1\mathcal{K}_1 \to \mathcal{R}_1\mathcal{K}_1\mathcal{R}_3, \quad \lim_{t\to\infty} \mathcal{R}_1\mathcal{K}_1\mathcal{R}_3 = \mathcal{R}_1\mathcal{R}_3. \tag{6.10}$$

(c) When $m_r - m_0 > \delta_7(m_l, m_0)$, $\boldsymbol{v}_r \in B$. The shock $S_1(\boldsymbol{v}_0, \boldsymbol{v}_r)$, where the bracket now indicates that the 1-S shock joins a state $\boldsymbol{v}_0$ on the left and $\boldsymbol{v}_r$ on the right in (ξ, t)-plane, is strong compared to the simple wave $R_1(\boldsymbol{v}_l, \boldsymbol{v}_0)$ and hence traverses through this simple wave in finite time. The diagram in (m, θ)-plane, which we have been using so far, does not describe the process of interaction but from our understanding of shock propagation we can describe qualitatively the process of interaction. When the 1-S shock overtakes from the right the trailing end of the 1-R wave, a 3-R wave (reflected wave) starts getting generated. The 1-S shock becomes weaker (note $m_0 < m_l$ so that $m_r - m_0 > m_r - m_l$) and after the completion of the interaction in finite time, it joins the state $\boldsymbol{v}_l$ on the left and a new constant state $\boldsymbol{v}_i$ on the right. The 3-R wave generated by the interaction is $R_3(\boldsymbol{v}_i, \boldsymbol{v}_r)$. The final result is given by the position of $\boldsymbol{v}_r \in B$ in (m, θ)-plane. We have shown the result (in (ξ, t)-plane) in Fig. 6.1. Symbolically the result is represented by

$$\mathcal{R}_1\mathcal{K}_1 \to \mathcal{K}_1\mathcal{R}_3, \tag{6.11}$$

which has been presented in detail in Fig. 6.2.

(viii) $\mathcal{K}_1\mathcal{R}_1$ **interaction:** Here $\boldsymbol{v}_0 \in S_1^+(\boldsymbol{v}_l)$ and $\boldsymbol{v}_r \in R_1^-(\boldsymbol{v}_0)$. We have observed from extensive numerical computation that the curve $R_1^-(\boldsymbol{v}_0)$ is above the curve $S_1^+(\boldsymbol{v}_l)$. Then there exists a function $\delta_8(m_l, m_0)$ such that when $m_0 - m_r = \delta_8(m_l, m_0)$, the state $\boldsymbol{v}_r \in R_3^+(\boldsymbol{v}_l)$. As in the last case, three cases arise.

(a) When $m_r > m_0 - \delta_8(m_l, m_0)$, the point $\boldsymbol{v}_r$ is in the domain B and we get the result

$$\mathcal{K}_1\mathcal{R}_1 \to \mathcal{K}_1\mathcal{R}_3. \tag{6.12}$$

The kink $\mathcal{K}_1$ is sufficiently strong to annihilate the elementary shape $\mathcal{R}_1$. The new elementary shape $\mathcal{R}_3$ produced as a result of the interaction is separated from the kink $\mathcal{K}_1$ by a straight portion represented by a constant state $\boldsymbol{v}_i$.

(b) When $m_r = m_0 - \delta_8(m_l, m_0)$, as in the case (vii)-(a), the kink $\mathcal{K}_1$ annihilates the elementary shape $\mathcal{R}_1$ in infinite time but asymptotically the strength of the kink $\mathcal{K}_1$ also

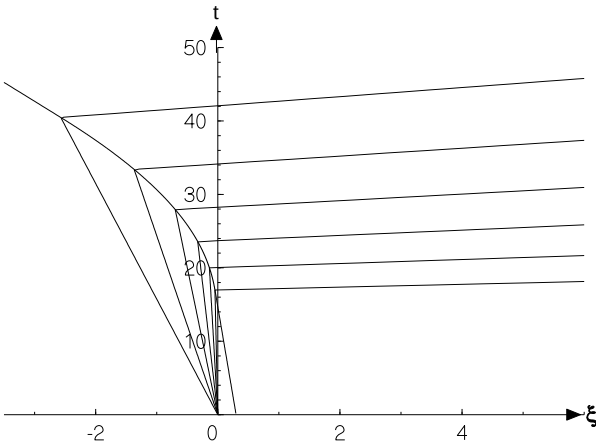

Fig. 6.1: *Pre-image of the $\mathcal{R}_1\mathcal{K}_1 \to \mathcal{K}_1\mathcal{R}_3$ interaction in (ξ, t)-plane when $m_r - m_0 > \delta_7$. The straight line characteristic curves in R_1-wave and those in R_3 are shown in the figure.*

vanishes as $t \to \infty$. Thus we get

$$\mathcal{K}_1\mathcal{R}_1 \to \mathcal{K}_1\mathcal{R}_1\mathcal{R}_3, \quad \lim_{t\to\infty} \mathcal{K}_1\mathcal{R}_1\mathcal{R}_3 = \mathcal{R}_3. \tag{6.13}$$

(c) When the elementary shape $\mathcal{R}_1$ is sufficiently strong, there exists a function $\delta_8'(m_l, m_0)$ such that for $m_0 - m_r = \delta_8'(m_l, m_0)$, the state $\boldsymbol{v}_r$ is on the curve T. For $m_0 - \delta_8'(m_l, m_0) < m_r < m_0 - \delta_8(m_l, m_0)$, the point $\boldsymbol{v}_r \in A$. The kink $\mathcal{K}_1$ is unable to annihilate the elementary shape $\mathcal{R}_1$ but in this process the strength of $\mathcal{K}_1$ tends to zero as $t \to \infty$ and we get the result

$$\mathcal{K}_1\mathcal{R}_1 \to \mathcal{K}_1\mathcal{R}_1\mathcal{R}_3, \quad \lim_{t\to\infty} \mathcal{K}_1\mathcal{R}_1\mathcal{R}_3 = \mathcal{R}_1\mathcal{R}_3. \tag{6.14}$$

(d) When $m_r \leq m_0 - \delta_8'(m_l, m_0)$, the point $\boldsymbol{v}_r \in T$ or the domain E. As discussed in (iv)-(b) and (c), we draw no conclusion.

(ix) $\mathcal{R}_3\mathcal{K}_3$ **interaction:** Here $\boldsymbol{v}_0 \in R_3^+(\boldsymbol{v}_l)$ and $\boldsymbol{v}_r \in S_3^-(\boldsymbol{v}_0)$. We see from numerical results that $S_3^-(\boldsymbol{v}_0)$ is above $R_3^+(\boldsymbol{v}_l)$. Now there exists a $\delta_9(m_l, m_0)$ such that if $m_0 - m_r = \delta_9(m_l, m_0)$, the point $\boldsymbol{v}_r \in R_1^-(\boldsymbol{v}_l)$. The following cases arise

(a) When the kink $\mathcal{K}_3$ is strong compared to the elementary shape $\mathcal{R}_3$ i.e., $m_0 - m_r > \delta_9(m_l, m_0)$, which implies $m_r < m_0 - \delta_9(m_l, m_0)$, the point $\boldsymbol{v}_r \in D$ and

$$\mathcal{R}_3\mathcal{K}_3 \to \mathcal{R}_1\mathcal{K}_3. \tag{6.15}$$

The interaction is of finite duration.

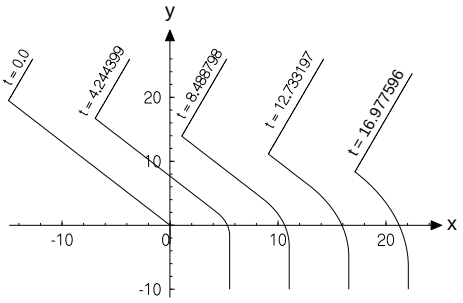

Fig. 6.2(a): *Up to the time of interaction.*

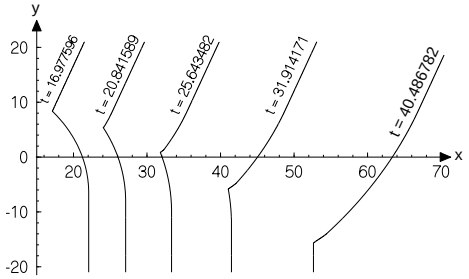

Fig. 6.2(b): *From initial to final time of interaction.*

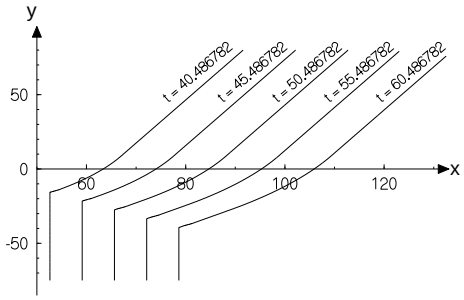

Fig. 6.2(c): *After interaction.*

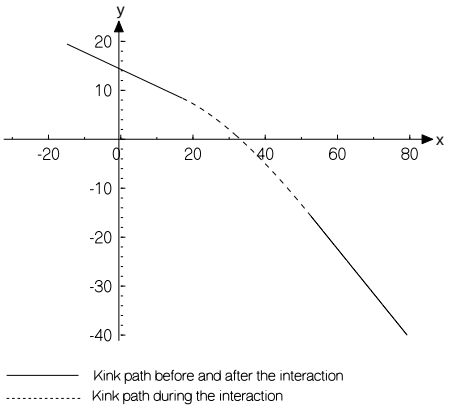

Fig. 6.2(d): *Kink path.*

Fig. 6: *The $\mathcal{R}_1\mathcal{K}_1$ interaction when $m_r - m_0 > \delta_7$*

(b) When $m_r = m_0 - \delta_9(m_l, m_0)$, the interaction between $\mathcal{K}_3$ and $\mathcal{R}_3$ continues indefinitely, both ultimately become infinitesimally weak and we have

$$\mathcal{R}_3\mathcal{K}_3 \to \mathcal{R}_1\mathcal{R}_3\mathcal{K}_3, \quad \lim_{t\to\infty} \mathcal{R}_1\mathcal{R}_3\mathcal{K}_3 = \mathcal{R}_1. \tag{6.16}$$

(c) When $m_r > m_0 - \delta_9(m_l, m_0)$, $\boldsymbol{v}_r \in A$. The interaction of $\mathcal{R}_3$ with $\mathcal{K}_3$ continues indefinitely during which process strength of $\mathcal{K}_3$ decays to zero and we get

$$\mathcal{R}_3\mathcal{K}_3 \to \mathcal{R}_1\mathcal{R}_3\mathcal{K}_3, \quad \lim_{t\to\infty} \mathcal{R}_1\mathcal{R}_3\mathcal{K}_3 = \mathcal{R}_1\mathcal{R}_3. \tag{6.17}$$

(x) $\mathcal{K}_3\mathcal{R}_3$ **interaction:** Here $\boldsymbol{v}_0 \in S_3^-(\boldsymbol{v}_l)$ and $\boldsymbol{v}_r \in R_3^+(\boldsymbol{v}_0)$. On the basis of numerical results, we accept that $R_3^+(\boldsymbol{v}_0)$ lies above $S_3^-(\boldsymbol{v}_l)$. Therefore, there exists a function $\delta_{10}(m_l, m_0)$ such that when $m_r - m_0 = \delta_{10}(m_l, m_0)$, the point $\boldsymbol{v}_r \in R_1^-(\boldsymbol{v}_l)$. We again get three cases.

(a) When $m_r < m_0 + \delta_{10}(m_l, m_0)$, $\boldsymbol{v}_r \in D$, the $\mathcal{K}_3$ annihilates $\mathcal{R}_3$ in finite time and we get

$$\mathcal{K}_3\mathcal{R}_3 \to \mathcal{R}_1\mathcal{K}_3. \tag{6.18}$$

(b) When $m_r = m_0 + \delta_{10}(m_l, m_0)$, we get

$$\mathcal{K}_3\mathcal{R}_3 \to \mathcal{R}_1\mathcal{K}_3\mathcal{R}_3, \quad \lim_{t\to\infty} \mathcal{R}_1\mathcal{K}_3\mathcal{R}_3 = \mathcal{R}_1. \tag{6.19}$$

(c) When $m_r > m_0 + \delta_{10}(m_l, m_0)$, $\boldsymbol{v}_r \in A$. We finally have

$$\mathcal{K}_3\mathcal{R}_3 \to \mathcal{R}_1\mathcal{K}_3\mathcal{R}_3, \quad \lim_{t\to\infty} \mathcal{R}_1\mathcal{K}_3\mathcal{R}_3 = \mathcal{R}_1\mathcal{R}_3. \tag{6.20}$$

Appendix: Equation for $\delta_4(m_l, m_0)$ when $\boldsymbol{v}_r \in T$.

Since $\boldsymbol{v}_0 \in \mathcal{R}_3^+(\boldsymbol{v}_l)$ with $\theta_l = 0$, and $\boldsymbol{v}_r \in \mathcal{R}_1^-(\boldsymbol{v}_0)$, we get

$$\theta_0 = \int_{m_l}^{m_0} \sqrt{\frac{-G'(m)}{mG(m)}}dm, \;\; \theta_r = \theta_0 + \int_{m_r}^{m_0} \sqrt{\frac{-G'(m)}{mG(m)}}dm.$$

On the other hand, since $\boldsymbol{v}_r \in T$, the expression of the curve T gives

$$\theta_r = \theta_+^* + \int_1^{m_r} \sqrt{\frac{-G'(m)}{mG(m)}}dm.$$

Since θ is monotonically increasing function of the curve T and is monotonically decreasing on $R_1^-(\boldsymbol{v}_0)$, these two curves will intersect at a unique point. This point of intersection can be obtained by equating the above two expressions for θ_r, which gives after simplification

$$\int_1^{m_r} \sqrt{\frac{-G'(m)}{mG(m)}}dm = \int_{m_l}^{m_0} \sqrt{\frac{-G'(m)}{mG(m)}}dm.$$

Once the function G is given explicitely, m_r can be obtained from the above expression and hence δ_4 can be calculated using the formula $\delta_4 = m_0 - m_r$.

Acknowledgemet: The authors express their sincere thanks to AR& DB, Ministry of Defence, Govt. of India for financial support through the project *Nonlinear Hyperbolic Waves in Multi-dimensions with Special Reference to Sonic Booms* (No. DRDO/08/1031199/M/I). They also thank Prof. S. Poedts for providing Phoolan Prasad a visiting position through a project No: OT/02/57.

Reference

1. Baskar, S and Prasad, P., (to appear), *Kinematical conservation laws applied to study geometrical shapes of a solitary wave*, in Wind Over Waves II: Forecasting and Fundamentals of Applications, ed., S. Sajjadi and J. Hunt, pp. 189 - 200.

2. K. W. Morton, P. Prasad and R. Ravindran (1992), *Conservation forms of nonlinear ray equations*, Tech. Rep., 2, Dept. Mathematics Indian Institute of Science.

3. Baskar, S., Potdar, N. and Szeftel (1999), Personal communication.

4. Courant, R and Friedrichs, K. O., (1948), *Supersonic flow and shock waves*, Interscience publishers (reprinted springer-verlog).

5. Monica, A and Prasad, P., (2001), *Propagation of a curved weak shock*, J. Fluid Mech., 434, pp. 119 - 151.

6. Prasad, P., (1995), *Formation and propagation of singularities on a non-linear wavefront and a shock front*, J. Indian Institute of Science, Special volume on Fluid Mechanics, 75, pp. 537 - 558.

7. Prasad, P., (1993), *Propagation of a curved shock and nonlinear ray theory*, Longman, Pitman Reearch Notes in Mathematics, 293.

8. Prasad, P and Sangeeta, K., (1999), *Numerical simulation of converging nonlinear wavefronts*, J. Fluid Mech., 385, pp. 1 - 20

9. Prasad, P., (2001), *Nonlinear hyperbolic waves in multi-dimensions*, Chapman and Hall/CRC, Monographs and Surveys in Pure and Applied Mathematics - 121.

10. Plotkin, K. J., (2001), *State of the art of sonic boom modeling*, J. Acoust. Soc. Am. 111(1), pp. 530 - 536.

11. Smoller, J., (1983), *Shock waves and reaction-diffusion equations*, Springer-verlog.

12. Sturtevant, B and Kulkarni, V. A., (1976), *The focusing of weak shock waves*, J. Fluid Mech., 73, pp. 651 - 671.

13. Whitham, G. B., (1974), *Linear and non-linear waves*, John Wiley and Sons.